PCM-modified textile-reinforced concrete slab: A multiscale and multiphysics investigation

Zakaria Ilyes Djamai, Khuong Le Nguyen, Amir Si Larbi, Ferdinando Salvatore, Gaochuang Cai

PCM-modified textile-reinforced concrete slab: A multiscale and multiphysics investigation

Zakaria Ilyes Djamai[1], Khuong Le Nguyen[2], Amir Si Larbi[3], Ferdinando Salvatore[3], Gaochuang Cai[3]

1-LMDC (Laboratoire Matériaux et Durabilité des Constructions), Université de Toulouse, INSA/UPS Génie Civil, 135 Avenue de Rangueil, 31077 Toulouse cedex 04, France.

2-Faculty of Civil Engineering, University of seven Transport Technology, Hanoi, Vietnam

3-Université de Lyon, Ecole Nationale d'Ingénieurs de Saint-Etienne (ENISE), Laboratoire de Tribologie et de Dynamique des Systèmes (LTDS), 58 Rue Jean Parot, 42000 Saint-Etienne, France

Corresponding author: djamai@insa-toulouse.fr

Abstract

This paper presents a multiphysics investigation of the effectiveness of textile-reinforced concrete (TRC) composite modified by the addition of phase change materials (PCMs).

The potential of this composite lies in the combination of the lightweight characteristic of TRC with the heat storage capacities provided by PCMs.

This study focuses on the effects of PCMs on both the mechanical and thermal performances of TRCs. The efficiency of an innovative concept of PCM–TRC slab resulting from the reinforcement of a PCM modified matrix with a textile grid is mechanically and thermally evaluated.

Despite the degradation of the mechanical performance of PCM–TRC slabs with PCM content, the ductile and multicracking behaviors of the slabs are conserved.

The temperature and thus the PCM state (solid or liquid) affect the mechanical performance of the PCM–mortar matrix and PCM–TRC slabs. This can be attributed to the PCM volume change that occurs during phase change.

In terms of thermal performance, in comparison with the reference TRC slab, the 10wt% PCM–TRC slab (4.5 cm thick) results in an energy saving of 37% and a temperature decrease of 4°C at the peak.

Key words

Phase change material (PCM), textile-reinforced concrete (TRC), mechanical behavior, thermal behavior, physicochemical investigation

1-Introduction

The building industry is one of the many consumers of energy. In the European Union, this industry accounts for 40% of the total energy consumption and 37% of the CO_2 emissions [1].

The use of renewable energy resources is crucial for improving building efficiency. In this context, the use of composite and non-conventional materials is increasing worldwide.

Textile-reinforced concrete (TRC) comprises a fine aggregate cementitious matrix reinforced with a non-corrosive textile fabric [2, 3]. TRC allows for the combination of compressive resistance and tensile strength due to textile reinforcement, thus enabling the construction of lightweight elements, such as sandwich and cladding panels [4, 5, 6, 7 and 8]. TRC exhibits a significant resistance to temperature (such as situations involving fire) and is considered as a promising alternative to fibre-reinforced polymers, which are characterised by their expensive cost, fire instability, and toxicity [6]. Despite these benefits, the reduced thickness of TRC structures (which are lightweight because of the reduced covers attributed to the non-corrosive fabric) can lead to the degradation of thermal inertia, thus limiting the possibilities of current construction applications.

Although sensible heat storage is the most exploited in the construction industry owing to the wide range of building materials, such as concrete and cellular foams, latent heat storage with the incorporation of phase change materials (PCMs) is of growing interest in the scientific community. PCM can reduce the indoor temperature variation by absorbing and releasing the latent heat generated by a phase change in a narrow temperature range [9, 10]. When the temperature is above the phase change temperature, the PCM melts and absorbs energy that can be restored when the PCM solidifies at a temperature below the phase change temperature.

The incorporation of PCM in cementitious materials, such as concrete, has received significant attention from researchers through different techniques, such as direct incorporation [11, 12], shape stabilisation [13], and vacuum impregnation [14]. However, the encapsulation technique [15, 16, 17, 18, 19, and 20] is the most suitable for preventing leakage of pure PCM wax.

Several researchers have investigated the incorporation of encapsulated PCM in concrete to achieve thermal comfort in the building envelope. Some researchers [19, 21, 22, and 23] studied the energy saving of PCM-concrete without analysing the effect of PCM on the microstructure and mechanical behaviour of concrete. Other researchers [24, 25] focused more on the mechanical behaviour of PCM-concrete structures without evaluating the effect of PCM on thermal performances. Other research studies [26, 27] focused on the effect of PCM on the mechanism of cement hydration and its consequences on the microstructure of concrete.

Castellon [19] constructed two identical cubicles (with walls having a 12-cm thickness) composed of plain concrete and PCM-modified concrete containing 5wt% PCM. These cubicles were located in the south of Spain and were exposed to the atmosphere. The PCM–concrete cubicles demonstrated a peak temperature attenuation of 4°C with a peak delay time of 4 h. Hunger [20] observed a 12% energy saving using self-compacting concrete containing 5wt% microencapsulated PCM when subjected to cyclic thermal loading. Although the thermal benefits of PCM addition in concrete have been verified in the literature [21, 22], negative effects of PCM addition are also observed in the mechanical performance of PCM-concrete [24, 25, 26, 27, 28]. In addition, the high costs of the PCM encapsulation process, as well as steel reinforcement, lead to uncompetitive steel-reinforced PCM concrete, which further hinders the introduction of PCM concrete in the construction market. Furthermore, PCM can significantly increase the porosity and critical pore diameter of concrete [29], thereby reducing its durability, particularly in the case of an association with corrosive steel reinforcement.

The present study aims to enrich the state of the art on the effect of PCM addition on the thermomechanical behaviour of concrete and to combine the advantages of PCM-modified concrete and TRC to propose a new PCM-modified TRC composite 'PCM–TRC'. **The purpose of this study is to evaluate the efficiency of the proposed composite in structural elements, such as slabs.**

The concept of 'PCM-TRC slabs is interesting in many ways:

- The load-bearing slabs undergo heat. Therefore, the optimisation of heat transfer by PCM addition has an apparent interest.

- The flexural behaviour of the slabs allows optimum use of the textile reinforcement.

To this end, the innovative concept of a lightweight slab composed of PCM-modified concrete reinforced with a glass textile reinforcement (PCM–TRC slab) is evaluated in this study in terms of its mechanical behavior and thermal performance.

Unlike the effect of PCMs on the mechanical behavior of ordinary concrete, few studies have been conducted on the impact of PCM on the mechanical behavior of fibrous concrete and TRC structures. Savija et al [30] studied the effect of PCM on the resistance of PVA fibrous mortar. They observed that the addition of small amounts of microencapsulated PCM to fibrous mortar can reduce its compressive strength, while having a small effect on its flexural strength and deformation capacity.

Thus, the objective of this study is to **investigate the effect of PCM on the mechanical performance of PCM–TRC slabs**, particularly their bending response. This study uses a combination of mechanical tests and physicochemical investigations to explain the response of the slabs to different PCM rates.

Moreover, owing to the lack of research [31, 32] on the impact of the PCM state (solid or liquid) on the mechanical performance of PCM–mortar structures, this study focuses on the effects of temperature (and thus PCM state) on the mechanical performances of PCM–mortar matrices and their consequences on PCM–TRC slabs. The reasons for the changes in the PCM–TRC slabs responses due to temperature variations are also explained.

Finally, an experimental investigation is conducted to analyse the efficiency of the PCM–TRC slabs in terms of thermal performance and energy saving.

2-Material and methods

2-1 Materials

2-1-1 Cement mortar

A fine aggregate cement mortar (D<1.6 mm) was used in this study to ensure the adequate impregnation of the textile reinforcement for the 'PCM-TRC' slabs.

2-1-2 PCM material

The PCM used in the study was a fatty ester vegetal wax. The phase change temperature ranged from 24 to 27°C with a phase change peak at 25°C. The capacity of the PCM to store energy during phase change was 160 kJ/kg.

2-1-3 Textile reinforcement

The textile used in this study was a latex-coated AR glass fabric with a tensile resistance and Young's modulus of 800 ± 48 MPa and 53 ± 2.5 GPa respectively (informations provided by the producer). The textile grid has a mesh width of 4 mm and 5 mm in the warp and weft directions, respectively.

2-2 Experimental methods

2-2-1 Casting procedure

2-2-1-1 Production of the PCM- mortar matrices

PCM microcapsules were added at different 'rates' (i.e. the percentage of PCM per matrix weight) 0, 5, 10, 15wt% to the formulation of the cement mortar. A minimum rate of 5wt% is recommended to ensure a significant effect on the thermal efficiency [19].

Before fixing the PCM-mortar mixture compositions, a test of water absorption (table 1) after 24 hours of immersion in water was conducted according to EN 1097-6 [33] on the hydrophilic encapsulated PCM to evaluate the amount of water absorbed by 100 grams of PCM powder .

Mass of surface dried (24h in 100°C oven) PCM powder M_1(g)	Mass of saturated PCM powder after 24h immersion M_2 (g)	Water absorption coefficient ($\frac{M_2-M1}{M1}$) in %
100	154	54

Table 1 Test results of water absorption capacity of PCM powder

The high water demand of PCM [27, 34] is on the one hand due to its very high porosity and on the other hand attributed to the existence of –OH groups on the polymer shell used for microencapsulation. The -OH groups can induce chemical adsorption by creating hydrogen bonds.

The high hydrophilic nature of PCM impairs the workability of concrete. This implies an adjustment of the $\frac{total\ water}{cement}$ ratio at each PCM rate to achieve equivalent conditions of impregnation of textile reinforcement in the PCM-TRC composites at each PCM rate.

However, it should be emphasized that since additional water in each PCM-mortar formulation is fully attributed to PCM absorption, a constant ratio of $\frac{water\ not\ absorbed\ by\ PCM}{cement}$ is maintained in all the PCM-mortar formulations

It should also be emphasized, that a fine sand aggregate (0-1.2mm) has been chosen in the mix compositions of the PCM-mortar matrix to ensure good conditions of impregnation of the textile reinforcement which is characterized by a fine mesh opening (4mm×5mm).

The PCM–mortar mix compositions used for production of PCM-TRC slabs with the mortar raw materials densities are given tables 2 and 3, respectively (for 1 m^3 of each formulation).

PCM-mortars	Reference		5wt% PCM-mortar		10wt% PCM-mortar		15wt% PCM-mortar	
	Mass (kg)	Volume (dm^3)	Mass (kg)	Volume (dm^3)	Mass (kg)	Volume (dm^3)	Mass (kg)	Volume (dm^3)
Cement	450	143.30	450	143.30	450	143.30	450	143.30
PCM	0	0	103.89	111.72	185.47	199.43	249.5	268.28
Fine sand (0-1.2 mm)	1668.7	632.10	1254.97	475.37	904.62	342.66	604.05	228.81
Water	216	216	261	261	306	306	351	351
Superplasticizer	9	8.60	9	8.60	9	8.60	9	8.60
Mass fraction of PCM (%)	0		5		10		15	
Volume fraction of PCM (%)	0		11.17		19.94		26.82	
$\frac{\text{Total water}}{\text{Cement}}$	0.48		0.58		0.68		0.78	
$\frac{\text{Water not absorbed by PCM}}{\text{Cement}}$	0.48		0.48		0.48		0.48	
slump (mm)	182		181		182		183	

Table 2 PCM-mortar mixture compositions

Mortar components	PCM	Cement	Fine sand	Superplasticizer

Real density (kg/m^3)	930	3140	2640	1046

Table 3 Real density of mortar raw materials

<u>2-2-1-2 Production of the ‘PCM-TRC’ slabs</u>

One-third-scale PCM–TRC slab samples (600 × 600 × 45 mm) at different PCM rates (0, 5, 10, 15wt%) were realised using an insitu hand lay-up technique in plywood rigid moulds (**Figure 1**).

A suitable amount of each PCM–mortar matrix (0, 5, 10, 15wt% PCM) was spread on the bottom of the mould so that 4 mm cover layer was applied between the bottom textile reinforcement layer and the lower slab face. Then, the reinforcement was impregnated by the matrix with a roller such that the matrix penetrated the textile fabric meshes. The procedure was repeated so that the PCM–TRC slabs were reinforced with a textile layer every 5 mm thick in the in-tension area of the slab (the volumetric rate of reinforcement was 4.78%).

The slabs were tested using three-point bending. Special attention was given to the placement of the AR glass reinforcement in the area subjected to tensile stresses (the textile reinforcement was placed in the lower half of the slabs under the neutral axis).

Textile placement **Textile impregnation**

A- Insitu hand lay-up technique

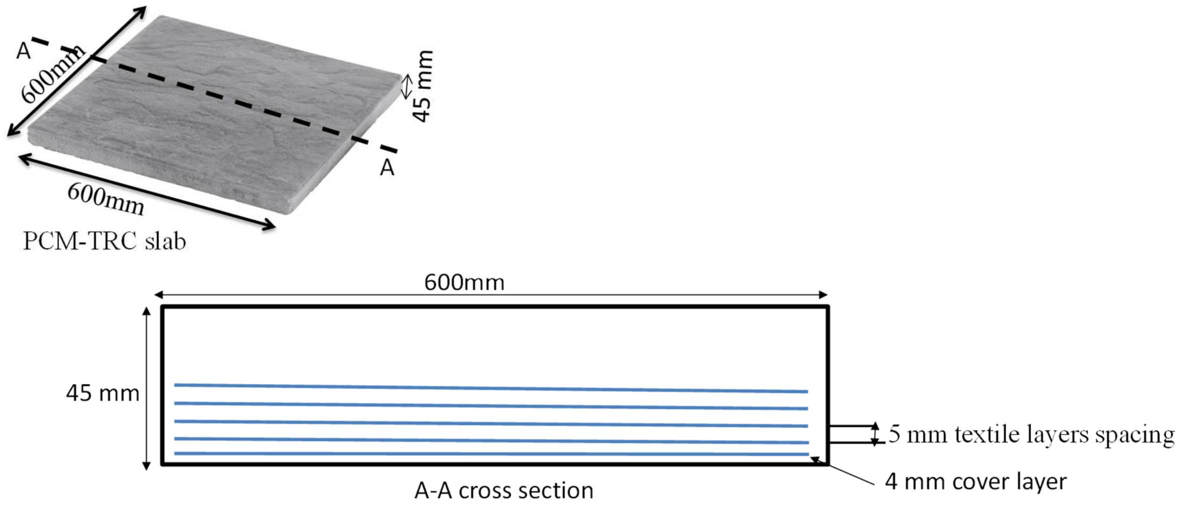

B- PCM-TRC slab A-A cross section with the textile renforcement

Figure 1 A- Insitu hand lay-up technique, B-PCM-TRC cross section

<u>2-2-2 Mechanical characterisation</u>

<u>2-2-2-1 Matrix scale</u>

<u>2-2-2-1-1 Mechanical behavior of PCM–mortar matrix at different PCM rates and temperature conditions</u>

Compression and bending tests were conducted on specimens containing 0, 5, 10, and 15wt% PCM with a loading speed of 2.4 kN/s for compression test and 0.015 mm/s for bending test according to EN 196-1[35] by considering two specimen temperatures: ambient temperature (maximum of 20°C) and a temperature of approximately 40°C. Five samples for each PCM rate and temperature condition were tested.

The samples tested at 40°C were placed for 6 h in an oven to induce a PCM phase change from solid to liquid. The tests were conducted 3 min after the samples were removed from the oven (five samples were tested for each PCM rate) to preserve the temperature homogeneity in the test samples.

A temperature of 40°C was chosen to be sufficiently high to ensure complete melting of the PCM and to limit the risk of temperature drop, which could lead to tests with the PCM in the liquid-to-solid transition phase. This temperature was also sufficiently low to ensure that the assumption of the absence of damage to the PCMs or mortar due to temperature before the tests was true. The age of the samples during testing was 28 days.

Five additional samples (of each PCM rate) were heated at 40°C then cooled to 20°C for 6 h in a temperature-conditioned room to allow homogeneous resolidification of the PCM. The tests on the heated then cooled samples were conducted 3 min after removing them from the temperature-conditioned room.

2-2-2-2 Structural element scale ('PCM-TRC' slabs)

2-2-2-2-1 Efficiency of textile reinforcement

To verify the effectiveness of textile reinforcement, three-point bending tests (**Figure 3**) with a loading speed of 0.2 mm/min, over a span of 570 mm, were conducted on a 600 × 400 × 45 mm unreinforced control slab without PCM and on a textile-reinforced slab without PCM (with a textile reinforcement rate of 4.78% in the in-tension zone). Three samples per specimen configuration were evaluated.

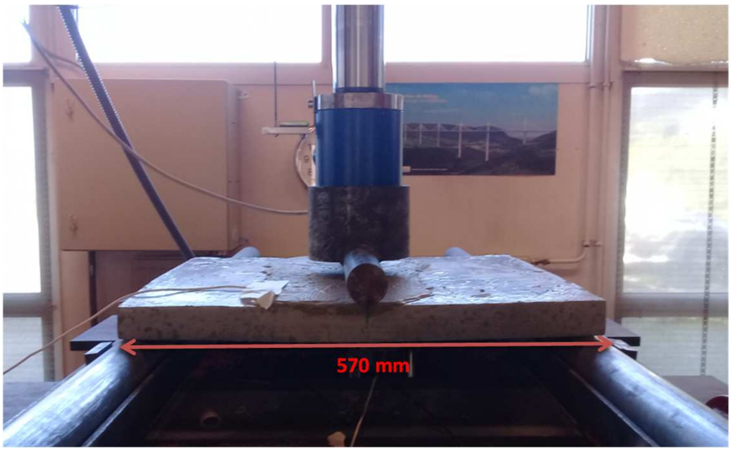

Figure 3 Three points bending test on PCM-TRC slab

2-2-2-2-2 Mechanical tests at variable PCM rate and constant temperature

PCM-TRC slabs (600×400×45mm) at different PCM rates (0, 5, 10 and 15wt%) were tested in displacement imposed three points bending with a loading speed of 0.2 mm/min and over a span of 570 mm

The temperature during the tests was maintained at 20°C (the PCM incorporated in the slabs is therefore in the solid state).

Three slabs per PCM rate were tested during this experimental campaign to ensure the reproducibility of the results.

The instrumentation used for the tests (**Figure 4**) comprised

1-An LVDT sensor vertically positioned at mid-span to measure the deflection of the slabs during the test.

2-Two LVDT sensors in a horizontal position to measure the elongation of the slabs in the in-tension face, over a measurement length of 200 mm. The first LVDT sensor was placed in the central zone of the in-tension face, and the second sensor was offset by 30 cm from the first.

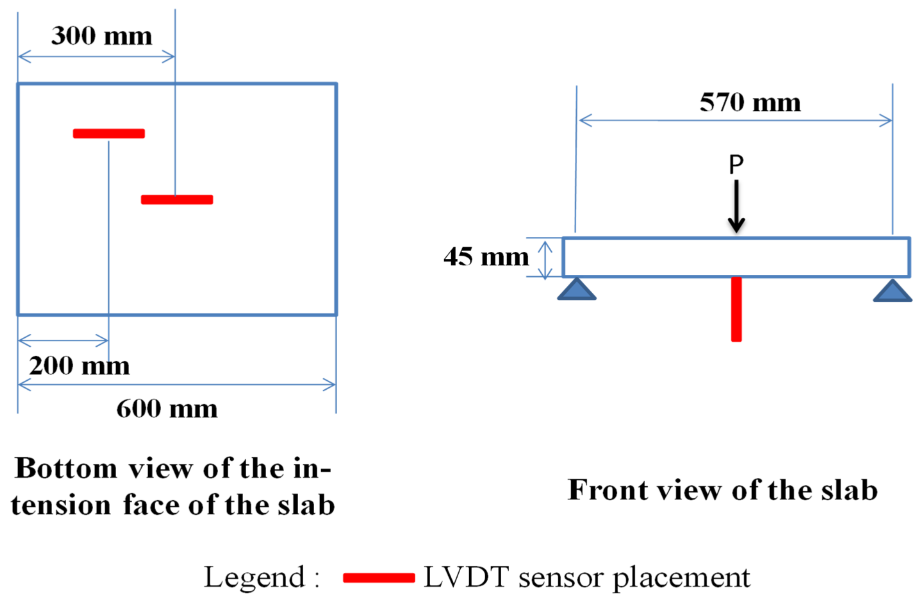

Figure 4 Instrumentation of bending tests on PCM-TRC slabs

2-2-2-2-3 Mechanical tests at variable temperature and constant PCM rate

The 10wt% PCM–TRC slabs with the same reinforcement rate (4.78%) underwent three-point bending tests under different temperature conditions to evaluate the effect of the PCM state on the mechanical performance of the PCM–TRC slabs (at the structural element scale). 10wt% PCM–TRC slabs at different temperatures were evaluated as described below:

A- A slab was maintained at 20°C and then underwent three-point bending tests at the same temperature

B- A slab was heated to 40°C for 6 h and then tested 3 min after being removed from the oven.

For sake of completeness, all the described tests section 2-2-2 are summarized **Table 4**

Type of test	Number of identical samples	Examined parameters
PCM-mortar compression and bending tests	5	- Strength at different temperatures - Rate of strength decrease due to PCM rate - Rate of strength decrease due to temperature - Rate of strength recovery due to temperature
PCM-TRC slabs bending tests at constant temperature and differents PCM rates	3	- Force at failure - Force at first crack - Deflection at failure - Textile exploitation ratio - Average crack spacing
PCM-TRC slabs bending tests at constant PCM rate and differents temperatures	2	- Force at failure - Force at first crack - Deflection at failure - Average crack spacing

Table 4 Summary of the examined parameters during the tests described section 2-2-2

2-2-3 SEM observations

To have a better understanding of the impact of PCM on the mechanical behavior of PCM–TRC slabs, SEM observations (on a MIRA FEG SEM) were conducted at the matrix/textile scale on a few samples of PCM–TRC composites at different PCM rates (the samples were realised beforehand for SEM observations). A backscattered electron detector was used to identify the different phases existing at the matrix/textile interface scale.

All the examined parameters are also summarized **Table 5**

Type of test	Number of identical simples	Examined parameters
SEM observation on PCM-TRC samples at matrix/textile interface	2	- Pore sizes at the matrix/textile interface - Matrix/textile interaction -Chemical characterisation (EDS analysis) at the matrix/textile interface

Table 5 Summary of the examined parameters during the SEM observation

2-2-4 Thermal performance evaluation

The thermal inertia of 1010 × 1010 × 45 mm PCM–TRC slabs was evaluated using a guarded hot box. The instrumentation during the test follows the recommendations of the standard ASTM C 236[36]. The guarded hot box comprised a hot-side enclosure, cold-side enclosure, and sample holder between the two enclosures where the test sample was placed (**Figure 5**). The same slab thickness used during the mechanical tests was considered for the thermal inertia test.

To evaluate the thermal inertia of the PCM–TRC slabs, similar scenarios were imposed on the reference slab (without PCM) and 10wt% PCM–TRC slab (slab with 10wt% PCM rate). The scenarios were as follows: first, the temperature was increased from 17 to 45 °C in 8 h on the hot side of the guarded hot box; second, the heating resistances in the hot chamber were turned off. The cold side remained free of any imposed stress throughout the entire scenario (see the imposed scenario **in Figure 5**). The aim was to analyse the effect of PCM addition on the air temperature and surface temperature of the slabs on the cold side. The imposed scenario corresponds to a situation wherein the hot side represents the outside temperature and the cold side represents the feeling inside a home.

Temperature sensors with a resolution of 0.1°C were positioned on the surfaces of the PCM–TRC slabs on the hot and cold sides of the samples. Two air temperature sensors were also positioned in each enclosure (on the hot and cold sides). The heat flux was measured thanks to the heat flux meters placed in the surface of the slabs in the two sides (in the hot and cold side of the guarded hot box).

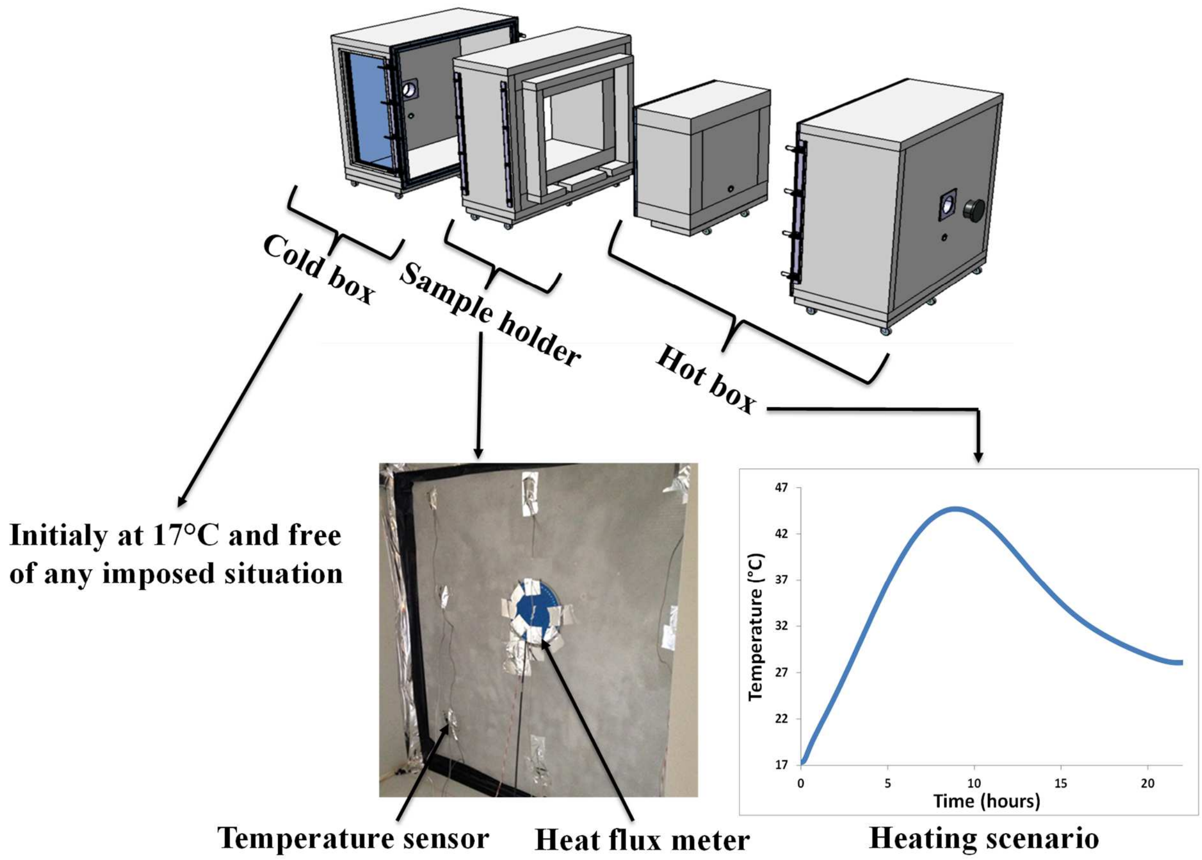

Figure 5 Imposed scenario in the guarded hot box for thermal inertia test on 'PCM-TRC' slabs

All the examined parameters during the test are summarized **Table 6**

Type of test	Number of identical simples	Examined parameters
Thermal inertia of PCM-TRC slabs	1	- Sample surface temperature in hot box - Air temperature in the hot box - Sample temperature in the cold box - Air temperature in the cold box - Heat flux in the hot and cold box - Stored energy by the sample

Table 6 Summary of the examined parameters during the thermal inertia test

3-Results and discussion

3-1 Mechanical characterisation

3-1-1 Matrix scale

3-1-1-1 Mechanical characterisation of PCM-mortar matrices

Figure 6 depicts compressive and tensile strength in bending of the 28-day matrices with different PCM rates. The tests were conducted under three temperature conditions: samples whose temperature was maintained at 20°C, samples heated to 40°C, and samples cooled to 20°C after heating at 40°C.

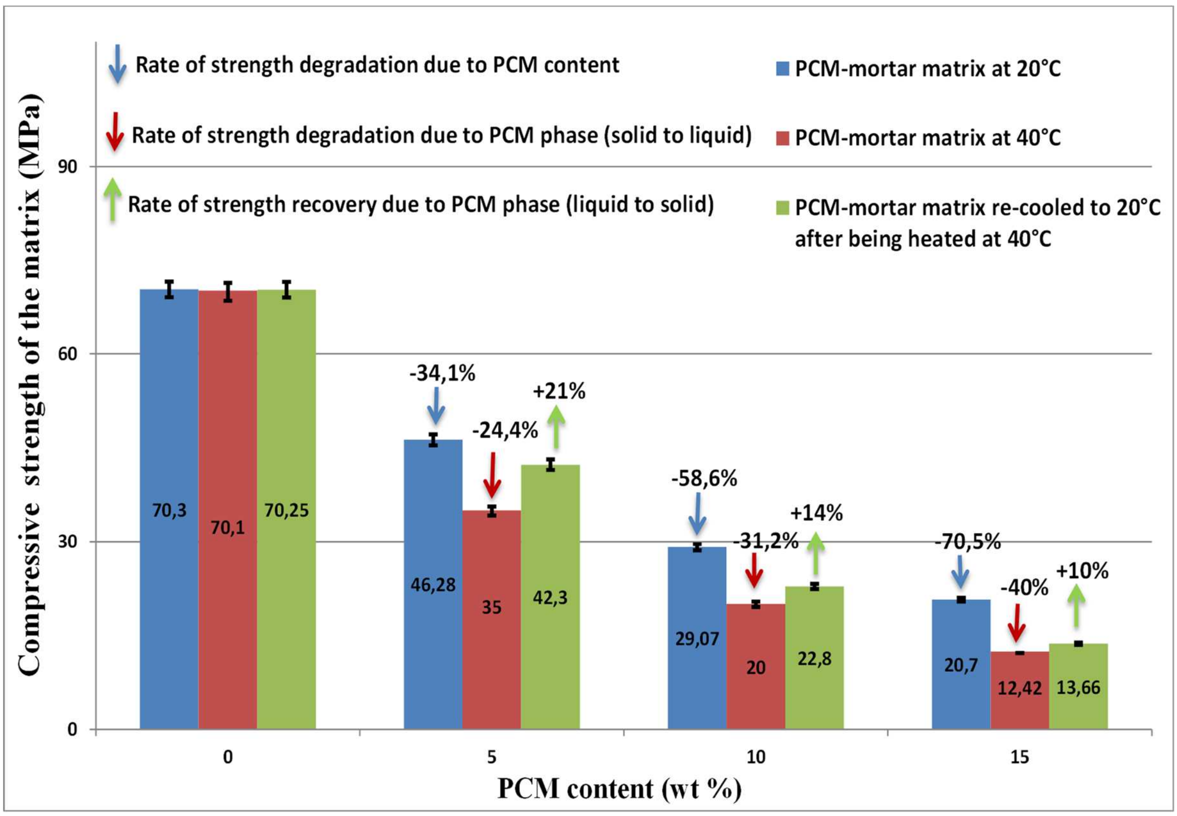

(a)

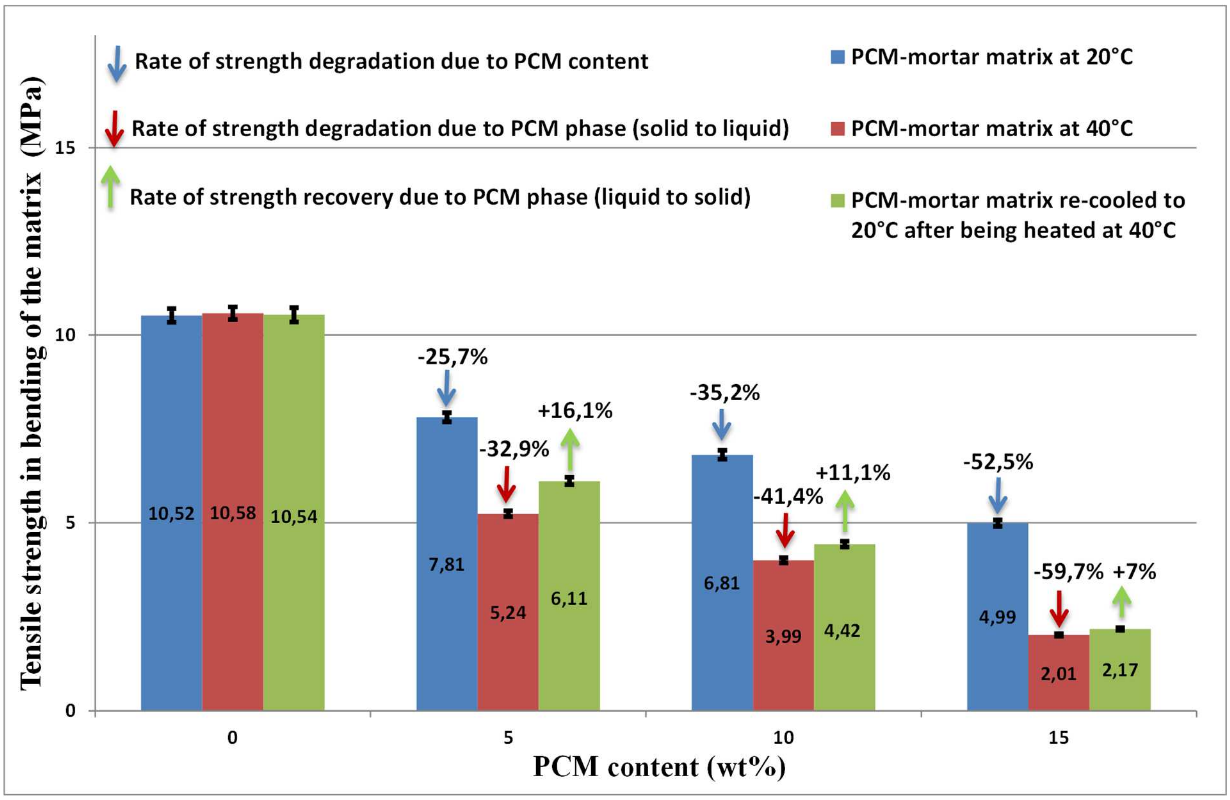

(b)

Figure 6 Effect of PCM rate and state on (a) the compressive strength (b) tensile strength in bending of PCM-mortar matrix

The main results derived from the experimental tests presented above are as follows:

(a)-The resistance of the PCM–mortar matrices decreased as the PCM rates increased during the mechanical tests of compression and bending. This observation was valid regardless of the temperatures.

(b) Significant degradation in the mechanical performance of the PCM–mortar matrices was observed when the PCM changed from the solid to liquid state after heating. The rate of strength deterioration increases when increasing PCM content in the matrices.

(c) Mechanical tests conducted on the PCM–mortar matrices cooled to 20°C after heating at 40°C for 6 h indicated that the initial strengths of the PCM–mortar samples were only partially restored.

Observations (b) and (c) can be attributed to the phenomenon of PCM expansion during phase change observed by the authors in [26, 33]. The transition from the solid to liquid state induces an increase in the PCM microcapsule volume, which can induce microcracking in the matrix (i.e. local strains). These microcracks are responsible for the degradation of the mechanical performance of the matrices and the partial restoration of the initial properties.

3-1-2 Structural element scale 'PCM-TRC slabs'

3-1-2-1 Efficiency of the textile reinforcement

The results of the three-point bending tests in terms of (force vs deflection) on unreinforced reference slabs (without PCM) and on reference slabs with a 4.78% rate of textile reinforcement in the in-tension area are depicted in **Figure 7**.

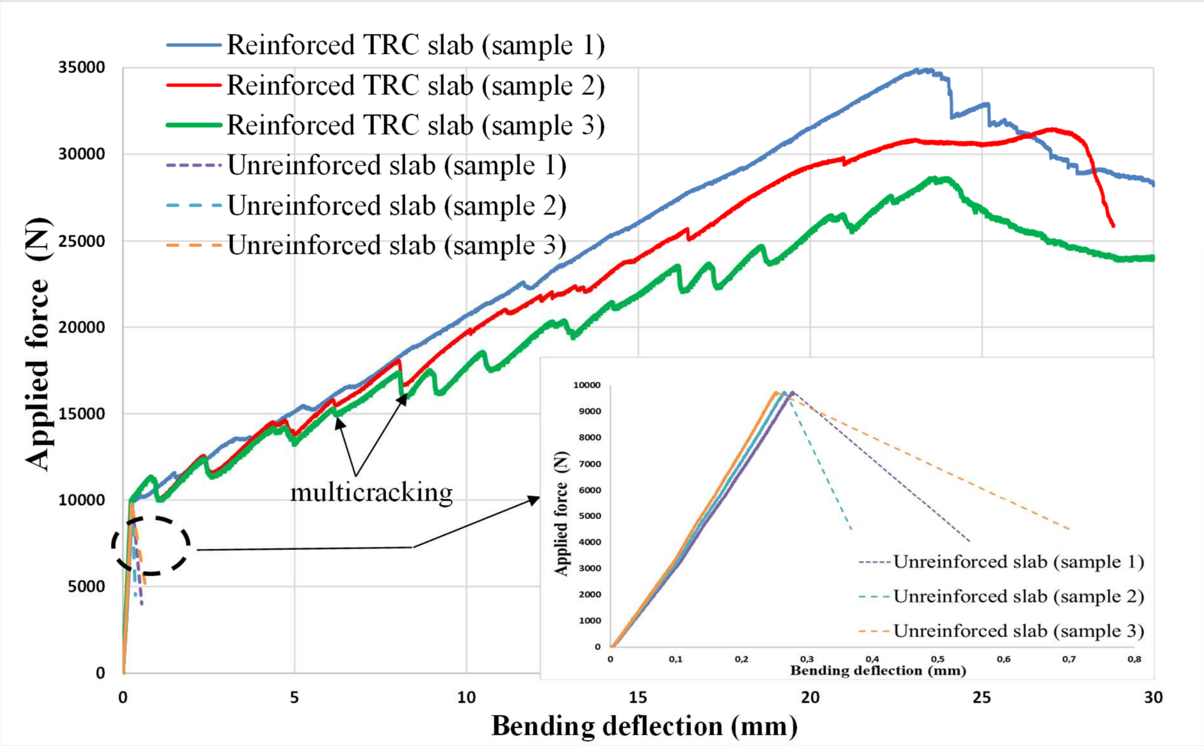

Figure 7 Three-point bending test result on reinforced and unreinforced slabs

The unreinforced slabs exhibited brittle behavior where the failure occurred directly after reaching the ultimate tensile stress of the mortar. A single macrocrack at mid-span followed by the simultaneous failure of the slab was observed (**Figure 8**).

In the reinforced slabs, a ductile and multicracking behavior was observed (see **Figure 8,** which depicts the cracking pattern in the in-tension area of the slab), synonymous to a matrix/textile stress transfer during the test. Failure of the reinforced slab occurred by compression crushing in the compressed face at mid-span.

Two distinct phases can be clearly identified in the reinforced slab (**Figure 7**). The first phase **(phase I, Figure 7)** corresponds to the elastic behavior of the slab. This phase ends at the occurrence of the first crack. The second phase **(phase II, Figure 7**) is associated with the change in slope on the force–deflection curve. This phase corresponds to the redistribution of forces from the cracked matrix towards the textile reinforcement at each crack in the in-tension area of the slab.

Brittle behaviour of unreinforced TRC slab | **Ductile and multicracking behaviour of reinforced TRC slab**

Figure 8 Behavior of reinforced and unreinforced slabs

3-1-2-2 Mechanical tests at variable PCM rate and constant temperature

3-1-2-2-1 Global behavior

The results of the three-point bending tests in terms of (force vs deflection) at a constant temperature of 20°C on the 0, 5, 10, and 15wt% PCM–TRC slabs are depicted in **Figure 9** (all experimentally derived curves for three samples per each PCM-TRC configuration are also presented **Appendix 1** at the end of the manuscript)**.** The main characteristics of the PCM–TRC slabs during the three-point bending tests are summarised in **Table 7.**

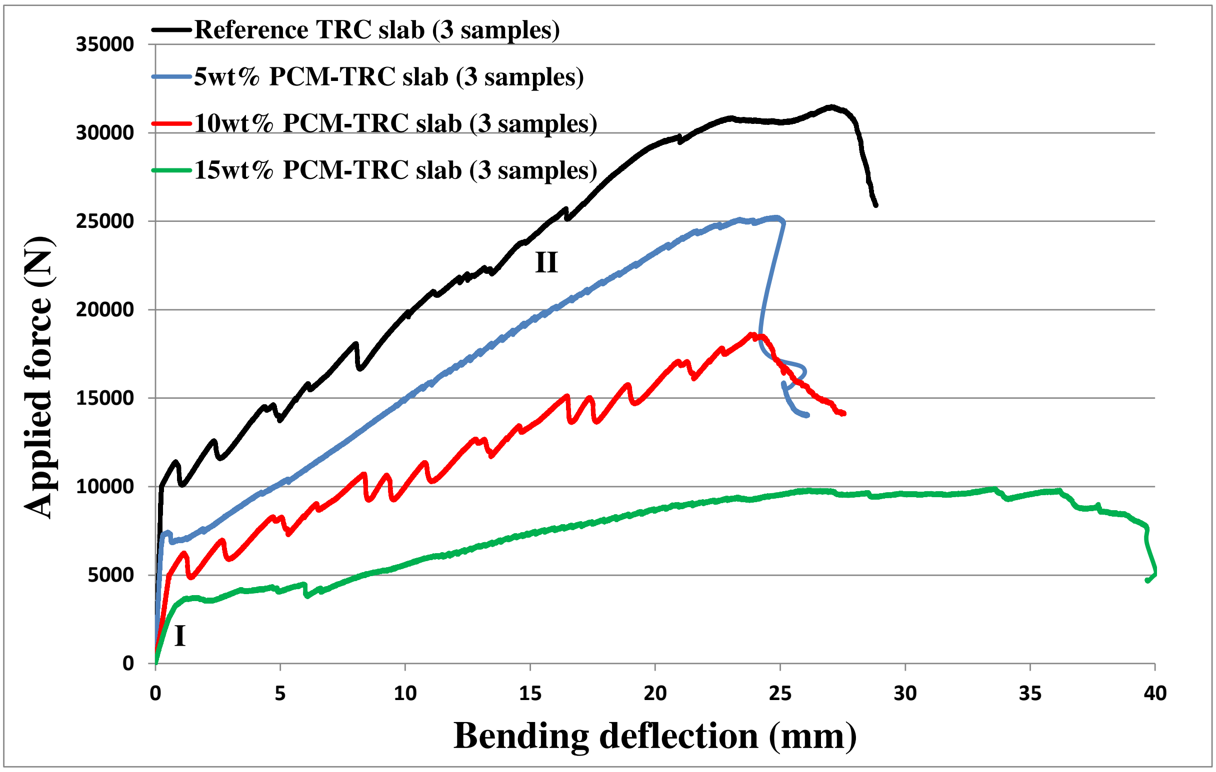

Figure 9 Bending test results on PCM-TRC slabs at different PCM rates (constant temperature)

PCM-TRC slabs	Unreinforced slab	Reference TRC slab	5wt% PCM-TRC slab	10wt% PCM-TRC slab	15wt% PCM-TRC slab
Force at first crack (kN)	9.8±0.4	9.76±0.4	7.2±0.3	4.7±0.2	2.9±0.12
Force at failure (kN)	9.8±0.4	31.6±1.9	25±1.7	19.7±1.2	9.9±0.5
Deflection at failure (mm)	0.4±0.1	23.9±0.8	23.3±0.7	23.9±0.7	36.1±2.8
Textile exploitation ratio (%)	/	82.12±3.5	72.98±3.0	48.38±2.3	27.88±1.9
Average crack spacing (cm)	/	2.0±0.1	2.65±0.1	3.7±0.1	5.1±0.1

Table 7 Performance characteristics of PCM-TRC slabs during bending test

From the results presented in **Figure 9** and **Table 7**, it can be seen that the load-bearing capacity of the slabs decreases with the increase in the PCM rate.

By analysing the force–deflection curves in detail, it can be deduced that

- The elastic phase I (phase I in **Figure 9**) is characterised by a degradation in the mechanical performance (force at first crack and bending rigidity) of the PCM–TRC slabs with the increase in the PCM rate, in accordance with **Section 3-1-1**. In fact, the mechanical performance of the slabs in phase I is mainly dependent on the mechanical performance of the PCM–mortar matrices, which is degraded by the increasing amount of PCM.

- In the textile contribution phase II (phase II in **Figure 9**, which begins at the occurrence of the first crack and ends at failure), the load is transmitted progressively from the matrix to the textile reinforcement at the occurrence of each crack. It can be observed that the 0, 5, and 10 wt% PCM–TRC slabs exhibit almost identical deflections at failure**, whereas the 15wt% PCM–TRC slab** exhibits a greater deflection. This is explained by the particular mode of failure of the latter. In fact, the mode of rupture of the 15wt% PCM-TRC slab is due to inferior matrix-to-textile bond conditions that induced textile slippage from the matrix leading to larger deflections and a deeper compression zone (**Figure 10**). Conversely, the failure modes of the 0, 5, and 10wt% PCM–TRC slabs occur due to a sudden compression crushing of the matrix (**Figure 10**).

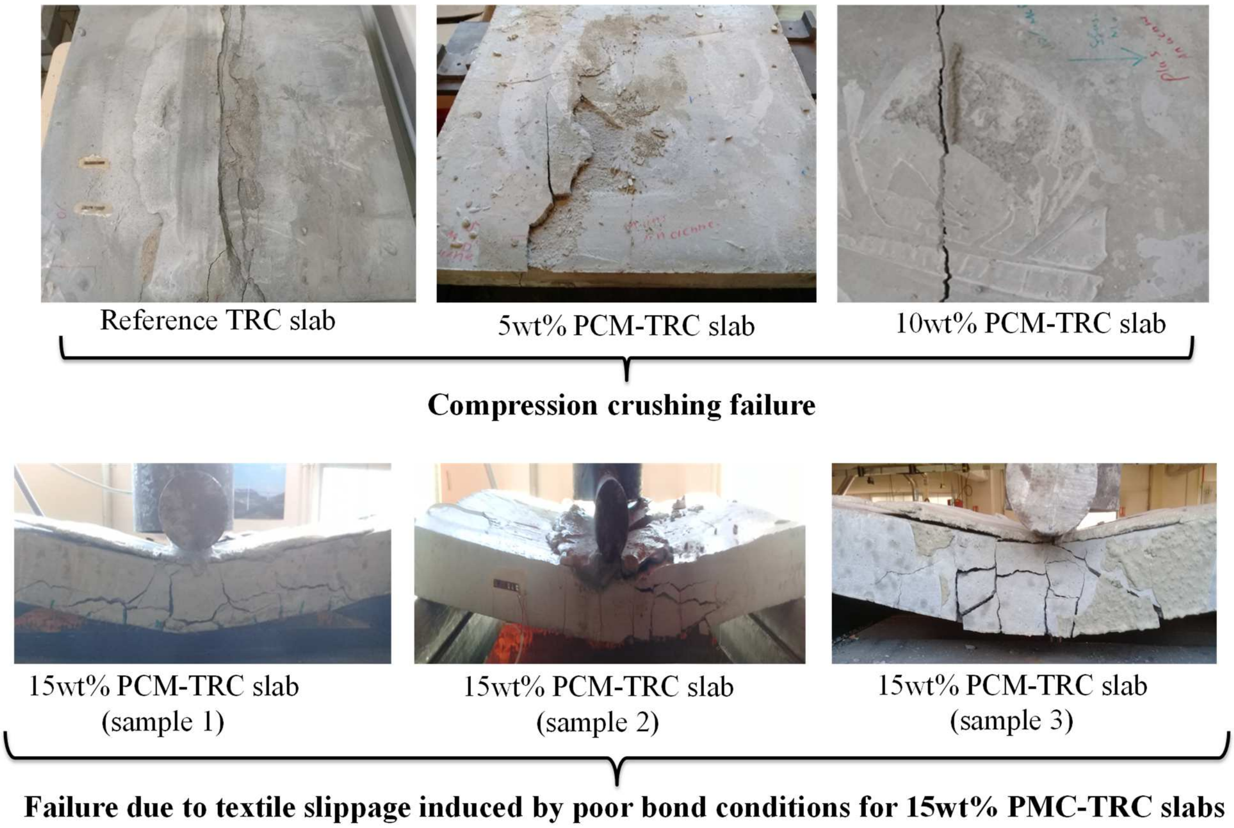

Figure 10 Failure modes of PCM-TRC slabs in bending tests at constant temperature

<u>3-1-2-2-2 Local behaviour (LVDT sensors and crack spacing)</u>

The graph of the (force vs longitudinal axial strain) and (Tensile stress in the in-tension part of the section of the slabs vs longitudinal strain) in the mid-span area is illustrated in **Figure 11** (obtained by the LVDT sensor placed in the central zone of the in-tension face, **Section 2-2-2-2-2**).

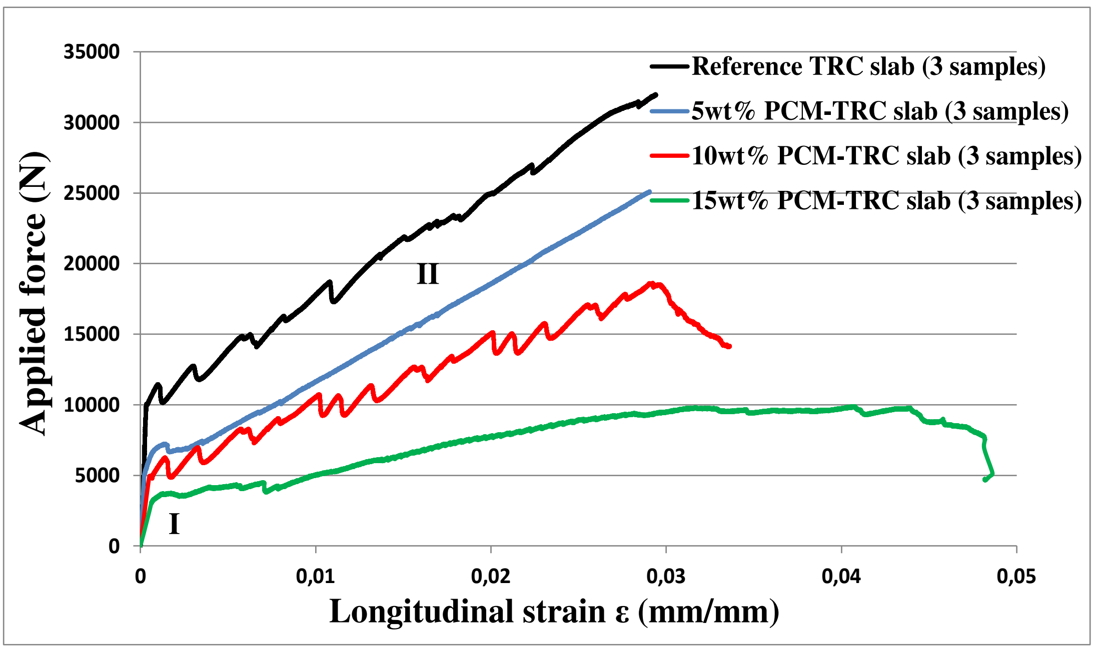

(a)

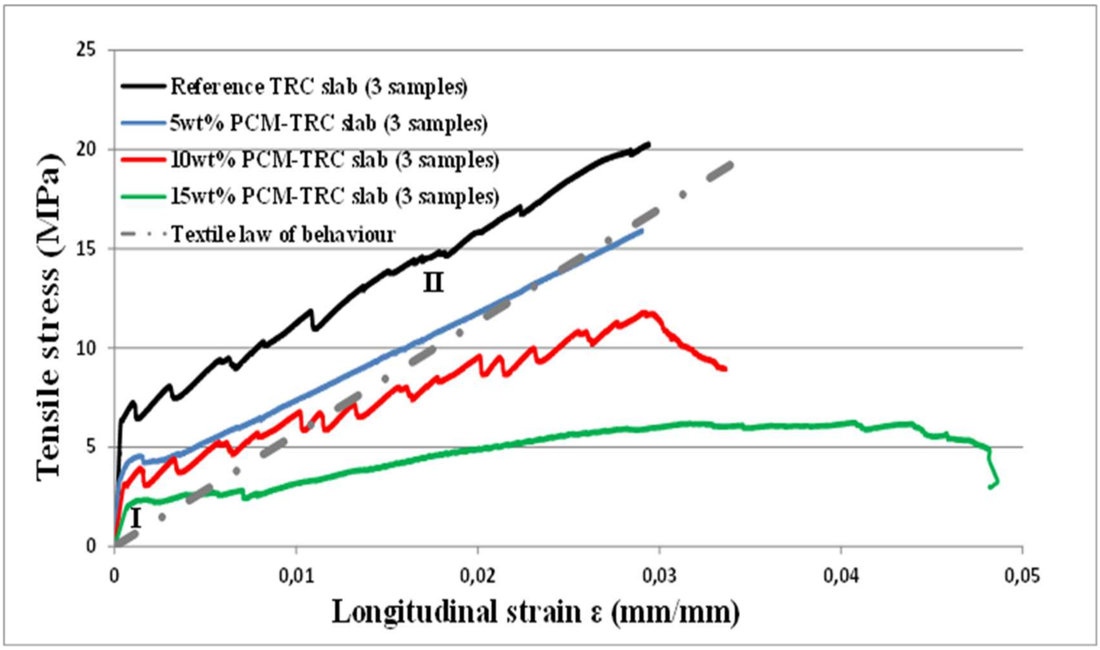

(b)

Figure 11 (a) Force vs longitudinal strain at mid-span (b) Tensile stress in the in-tension part of the section at mid-span

The curves are divided into two phases:

Phase I with high rigidity corresponding to the evolution of the strain of the uncracked matrix

Phase II is characterised by a significantly lower rigidity corresponding to the strain evolution of the in-tension face during the phase of matrix multicracking and the matrix/textile load transfer at the occurrence of each crack. For the 15 wt% PCM, a higher strain at failure was observed, which can be explained by inferior matrix-to-textile bond conditions that induced textile slippage from the matrix (**Figure 10**). The LVDT sensors positioned in the in-tension face of the 15 wt% PCM–TRC slab measured the slip displacement of the interlaminar layer upon the occurrence of textile slippage, which explains the higher strain at failure for the 15 wt% PCM–TRC slab in comparison with those of the 0, 5, and 10 wt.% PCM–TRC slabs.

The textile slippage failure mode of the 15wt% PCM–TRC slab observed at the structural element scale is also consistent with the textile slippage rupture observed at the composite material scale in the tensile tests conducted by the authors [24, 32] on PCM–TRC composite samples at a PCM rate of 15wt%.

Figure 12 presents the textile exploitation ratio (textile work ratio) defined by the ratio $\frac{E_{II}}{E_{Textile}}$ (E_{II} represents the slop of the tensile stress vs strain in the phase II of figure 11-b , $E_{Textile}$ represents the textile modulus taking into consideration the textile volume ratio)

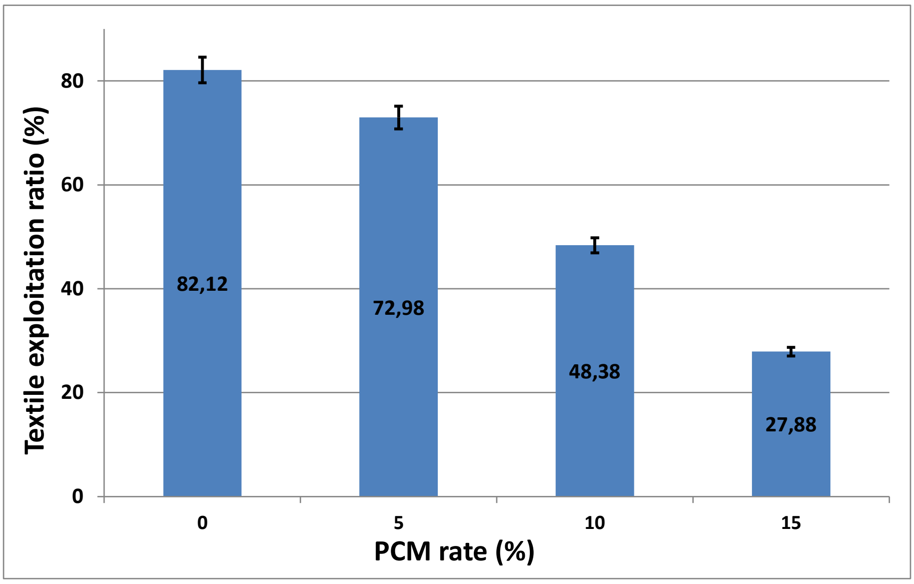

Figure 12 Evolution of the textile exploitation ratio with PCM rate

The textile exploitation ratio (textile work ratio) decreases with the PCM rate**.** This indicates a degradation in the intensity of the ‘matrix/textile’ interaction with the increase in the PCM content (degradation of the textile effectiveness).

It can also be seen from **Table 7 and Figure 13** that the average spacing between two consecutive cracks increases with the increase in the PCM rate. In other words, the total number of cracks decreases with the PCM content in the PCM–TRC slabs.

The average spacing between two consecutive cracks is directly related to the intensity of the matrix/textile interaction (more precisely, the matrix/textile contact surface area) as the appearance of a crack is synonymous to a matrix/textile stress transfer in the zone of crack apparition. Consequently, the matrix/textile stress transfer behavior increase with the increase in the number of cracks.

According to the crack spacing results **(Table 7 and Figure 13**), augmenting the PCM rate has a negative effect on the matrix/textile load transfer behavior. This confirms the analysis of the slope of the tensile stress–longitudinal strain curves in phase II **in Figure 11-b**. More clarifications on the effect of PCM on matrix/textile stress transfer behavior are provided in **Section 3-2**.

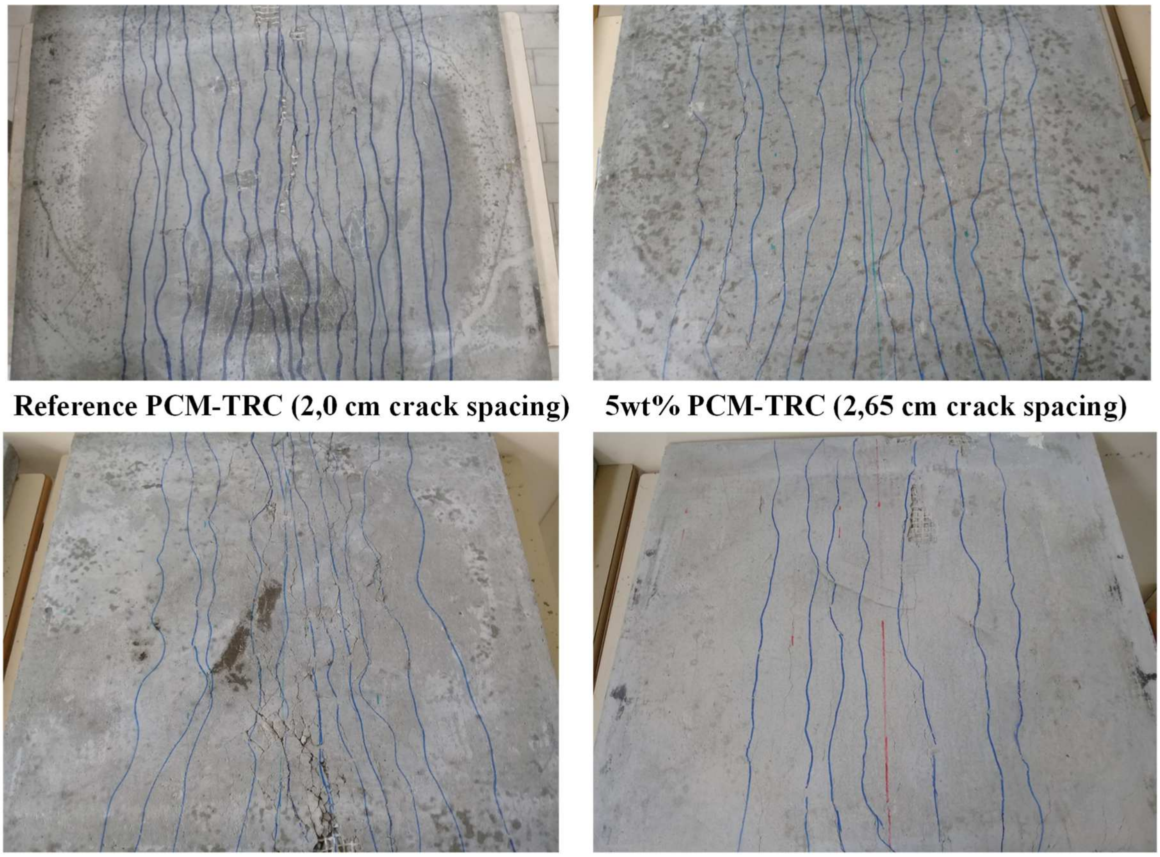

Reference PCM-TRC (2,0 cm crack spacing) **5wt% PCM-TRC (2,65 cm crack spacing)**

10wt% PCM-TRC (3,70 cm crack spacing) **15wt% PCM-TRC (5,10 cm crack spacing)**

Figure 13 Average crack spacing in the in-tension face for PCM-TRC slabs

<u>3-1-2-3 Mechanical tests at variable temperature and constant PCM rate</u>

Bending tests were conducted on 10wt% PCM–TRC slabs conserved at temperatures of 20 and 40°C, respectively.

The 10wt% PCM–TRC slab was selected for this test because it presents an optimum balance between its mechanical properties and thermal performance.

The results of the three-point bending tests in terms of (force vs deflection at mid-span and force vs axial deformation in the in-tension face at the mid-span area) on 10wt% PCM–TRC slabs maintained at 20°C and heated to 40°C are depicted in **Figures 14-a and 14-b.**

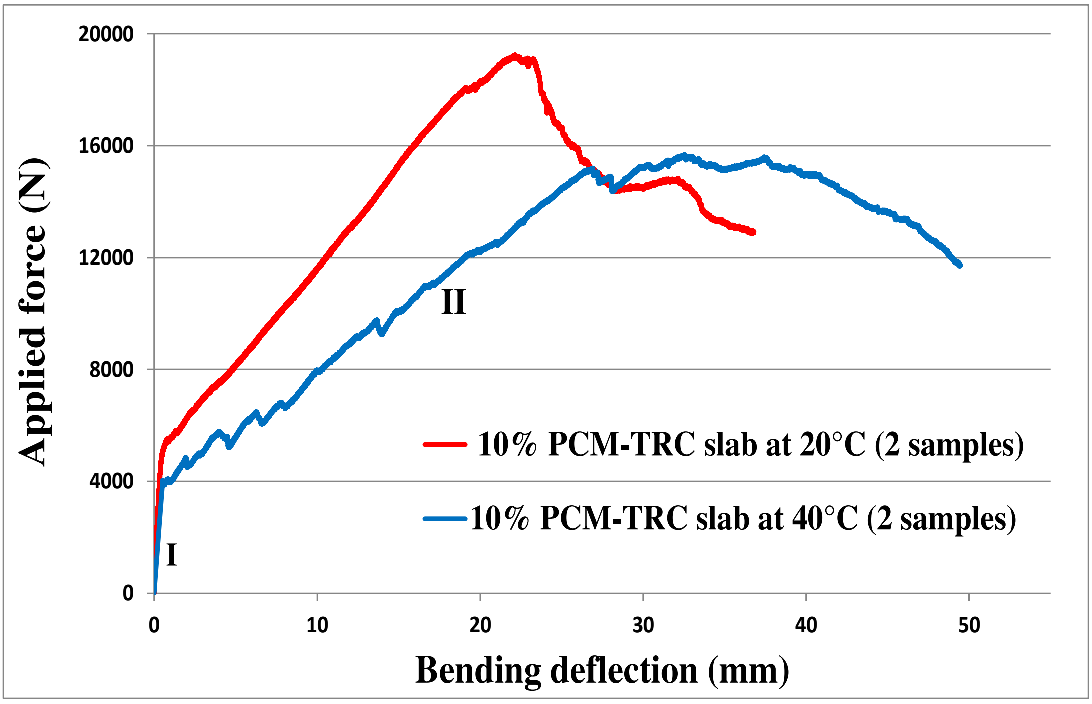

-a-

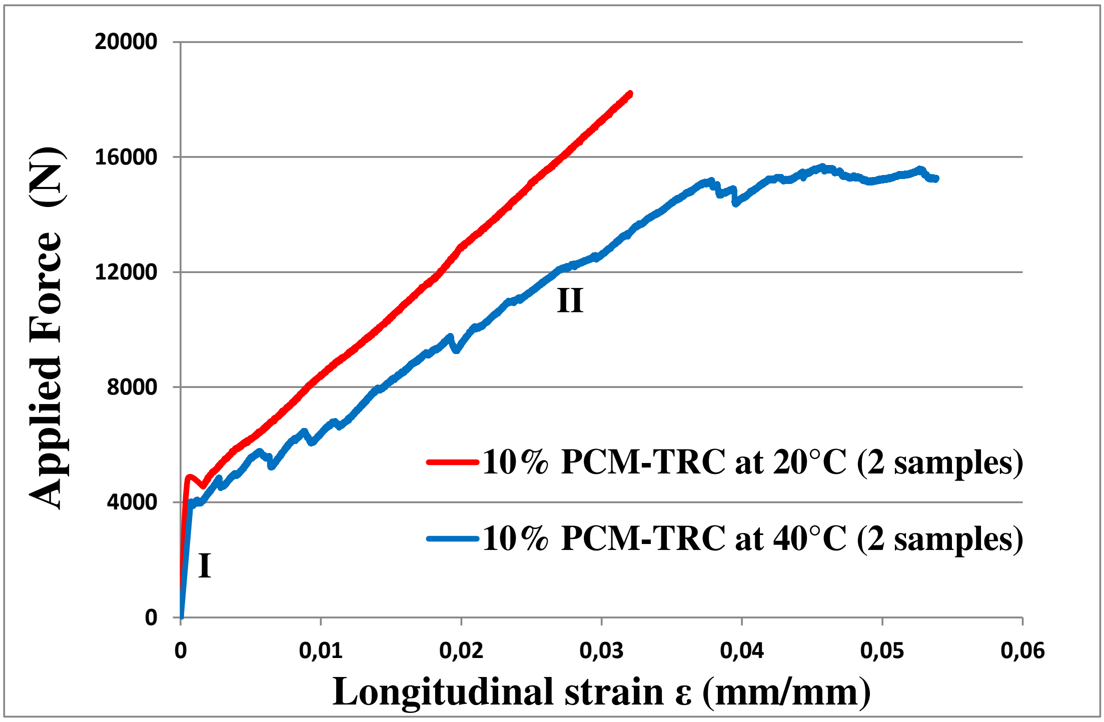

-b-

Figure 14 Effect of temperature on -a- force vs deflection and –b force vs strain (central zone)

The results depicted in **Figures 14-a and 14-b** indicate a slight decrease in the force at the appearance of the first crack (elastic phase), as well as a degradation of the load-bearing capacity of 21% for the 10wt% PCM–TRC slab heated to 40°C with respect to the slab maintained at 20°C. In addition, the failure mode of the slab heated to 40°C occurred by textile slippage initiated at the interlaminar space between the two lower textile reinforcement layers (**Figure 15**) at a force of 15000 N, whereas the failure mode of 10% PCM–TRC slabs maintained at 20°C occurred by compression crushing (**Figure 15**).

The textile slippage was confirmed by analysing the evolution of the longitudinal strain of the in-tension face at mid-span **(Figure 14-b),** wherein at a force of 15000 N, an increase in the strain is observed at an almost constant force for 10wt% PCM-TRC slab heated at 40°C. The measured strain during the delamination is due to the textile slippage caused by the degradation of the shear strength of the interlaminar layer (the layer between two textiles reinforcements) when PCM was at 40°C (the LVDT sensor placed in the in-tension face measures a parasitic deformation attributed to textile slippage).

A more detailed analysis of **Figure 14-b** also reveals a 30% decrease in the slope of the curve (force vs strain of the in-tension face at mid-span) in **phase II** for the 10wt% PCM–TRC slab heated at 40°C. This slope is directly proportional to textile reinforcement work ratio. The increase in the average crack spacing between two consecutive cracks in the in-tension faces for the slab heated at 40°C (average crack spacings of 3.6 cm and 4.3 cm for the 10wt% PCM–TRC slabs maintained at 20°C and heated at 40°C, respectively) confirms the deterioration of the matrix/textile interaction due to the effect of PCM state.

The degradation of the matrix/textile stress transfer (decrease in the textile work ratio 'textile efficiency ratio' in terms of stiffness) in addition to the weakening of the shear strength of the interlaminar layer (rupture by textile slippage) for the 10% PCM–TRC slab heated to 40 °C are most likely attributed to the effect of microcracking due to PCM expansion during its phase change. The microcracks at the matrix/textile interface can disturb the stress transfer from the matrix to the cracked interface until the textile reinforcement.

Compression crushing failure
10wt% PCM-TRC slab at 20°C

Delamination failure
10wt% PCM-TRC slab at 40°C

Figure 15 failure modes of 10wt% PCM-TRC slabs at different temperatures

<u>3-2 SEM observations</u>

It has been demonstrated in the previous sections that the addition of PCM induces mechanical performance degradation of the PCM–TRC slabs. The following SEM observations help further explain the effect of PCM on stress transfer at the matrix/textile interface.

3-2-1 SEM observation in a reference 'PCM-TRC' composite (without PCM)

Figure 16 depicts the SEM observation of longitudinal and transversal cross-sections at the matrix/textile interface in a reference TRC composite (without PCM).

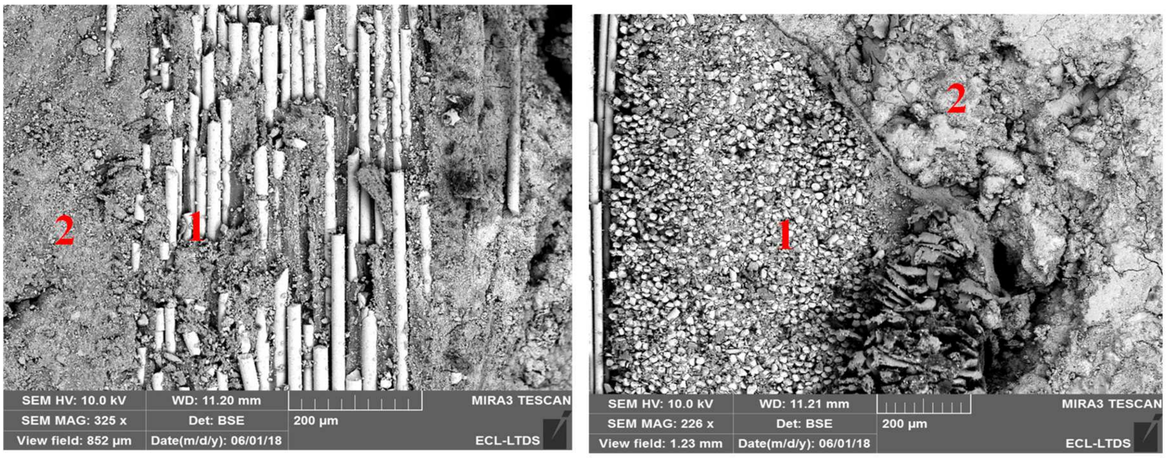

A- Longitudinal cross section

B- Transversal cross section

Legend: 1 Fiber yarn impregnated with latex, 2 matrix without PCM

Figure 16 SEM image of the reference TRC composite (without PCM)

A high degree of matrix/textile interaction can be observed. There is less porosity at the interface transition zone (ITZ) between the matrix and the fabric in the reference TRC (without PCM) compared to PCM-TRC composites (with the addition of PCM). In fact, SEM observation allows quantifying an ITZ spacing of 30 to 50 nm in the case of reference TRC composite while it varies between 1μm and 2 μm in function of the PCM rate in PCM-TRC composites **(Figure 17)**. This explains the high textile work ratio and the lowest average crack spacing observed for the reference TRC slab.

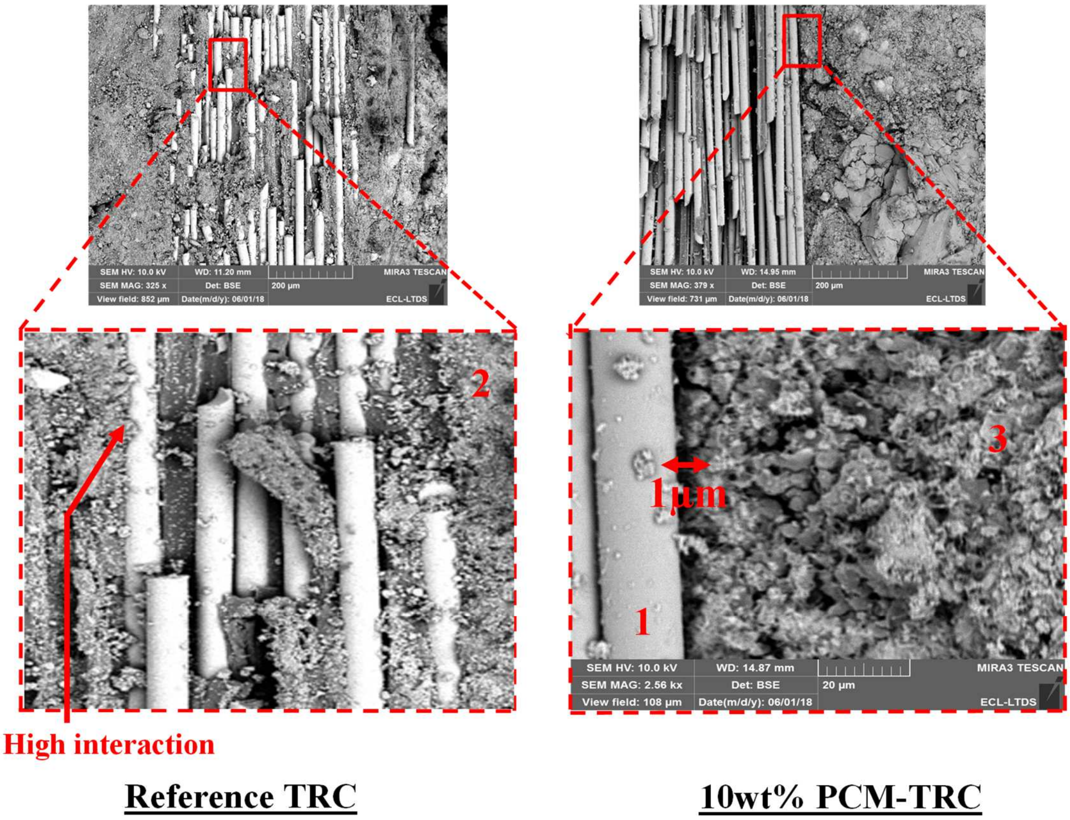

Legend: 1 Textile yarn, 2 matrix without PCM, 3 matrix with PCM inclusion

Figure 17 effect of PCM on ITZ ''matrix/textile' in PCM-TRC composites

3-2-2 SEM observations in the PCM-TRC composites (with PCM inclusions)

3-2-2-1 Effect of PCM on cement hydration in the proximity of the interface

Figure 18 depicts an SEM image of a 15wt% PCM–TRC composite that illustrates the consequences of the effect of PCM on the matrix hydration in the proximity of the matrix/textile interface.

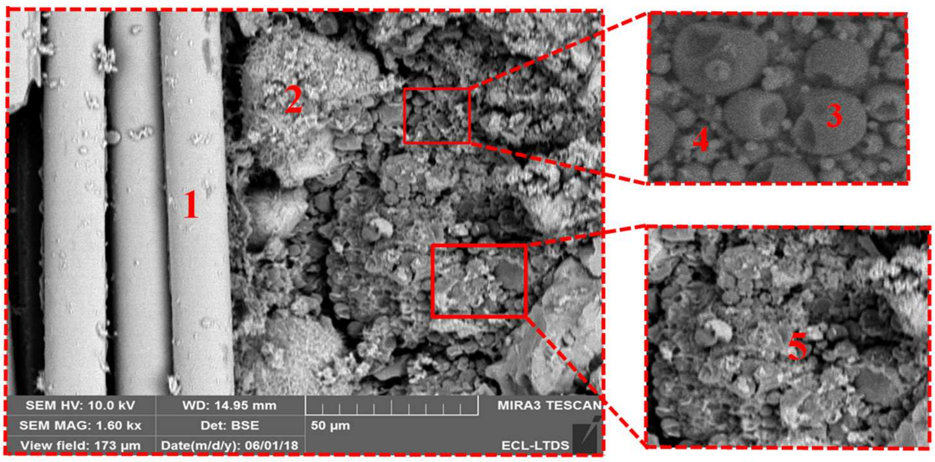

Legend : 1 Textile, 2 Cement, 3 PCM microcapsule, 4 nodules of pure PCM wax, 5 Agglomeration of PCM

Figure 18 SEM image illustrating the effect of PCM on cement hydration near the interface

From **Figure 18**, it can be observed that the chain of PCM capsules (**legend 3**) that surround the anhydrous cement **(legend 2)** in the immediate vicinity of the matrix/textile interface can inhibit its hydration by restricting its access to water, thereby reducing the amount of hydrated products from the cement in the interface zone. The consequence is a loss of the matrix/textile bond and a reduction of the textile exploitation ratio.

At the local scale of PCM, SEM observation also reveals that some damage may occur to the PCM microcapsules (**legend 3 in Figure 18**) inducing the leakage of pure PCM in the form of micronodules (**legend 4 in Figure 18**).

<u>3-2-2-2 Effect of PCM leakage at the interface proximity</u>

Figure 19 depicts another SEM observation of the 15wt% PCM–TRC composite, which demonstrates the effect of the deposition of large quantities of pure PCM wax (leaked from PCM capsules) in the immediate vicinity of the matrix/textile interface. The deposition of these quantities is illustrated in the framed area of **Figure 19** and confirmed by the EDS analysis that indicates the presence of an intense peak of carbon with a less pronounced peak of oxygen that are high probably attributed to pure PCM oil (CH_3-CH_2(14)-C(O)-O-CH_2). These quantities are most likely attributed to the damage of PCM microcapsules during the manufacture of the PCM–TRC composite using the hand lay-up technique. The progression of the CSH hydrate growth (**CSH gel is visible in legend 2 of Figure 19**) is inhibited in the deposition zone of the PCM oil in the proximity of the matrix/textile interface. This induces a decrease in the textile reinforcement work ratio (textile efficiency ratio).

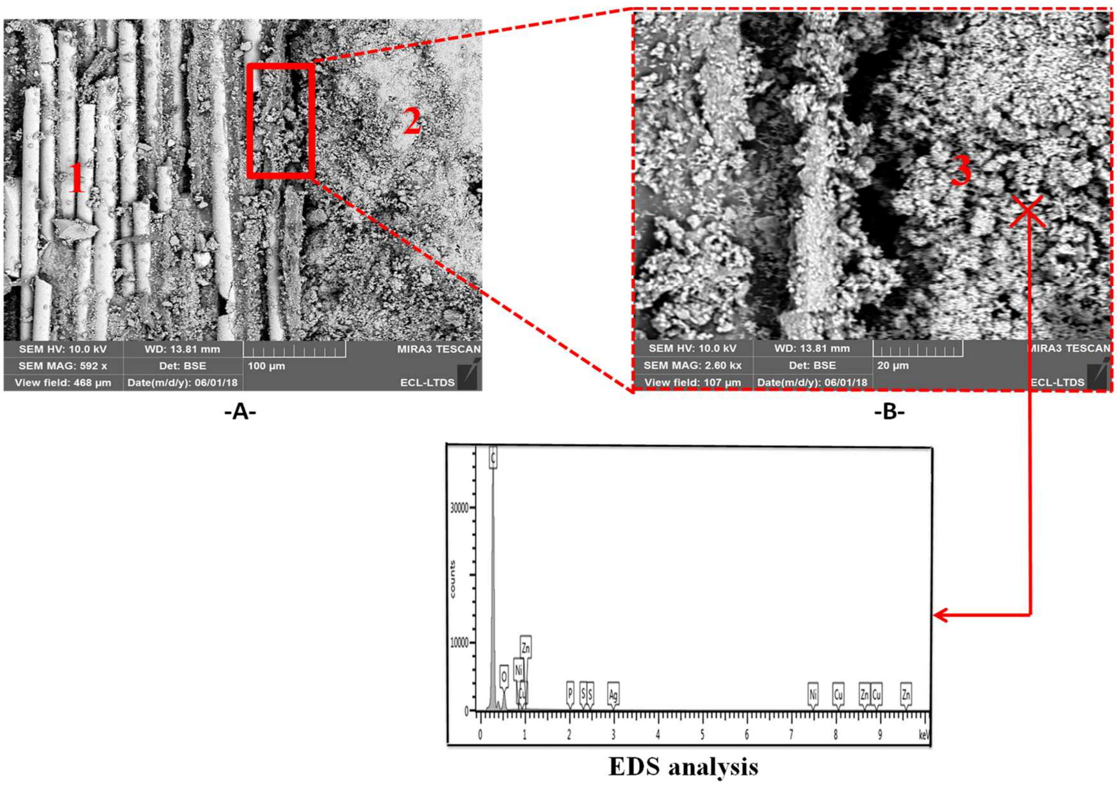

Legend : 1 Textile, 2 CSH hydrated product, 3 leaked PCM wax from damaged capsules

Figure 19 SEM image illustrating the effect of PCM wax leakage near the interface

3-3 Thermal performances of PCM-TRC slabs (result of thermal inertia test)

The results of the thermal inertia test (described in **Section 2-2-4**) on the reference TRC slab (without PCM) and 10wt% PCM–TRC slab (identified as the optimum balance between mechanical and thermal properties) in terms of the sample surface temperature and air temperature in the cold chamber are depicted in **Figures 20-a and 20-b**. Owing to the complexity of the instrumentation used and the sample scale, the authors specify that the results presented in this section are those obtained from a single test. The test scenario involved heating from 17 to 45°C in the hot chamber while the cold chamber remained free of any imposed condition.

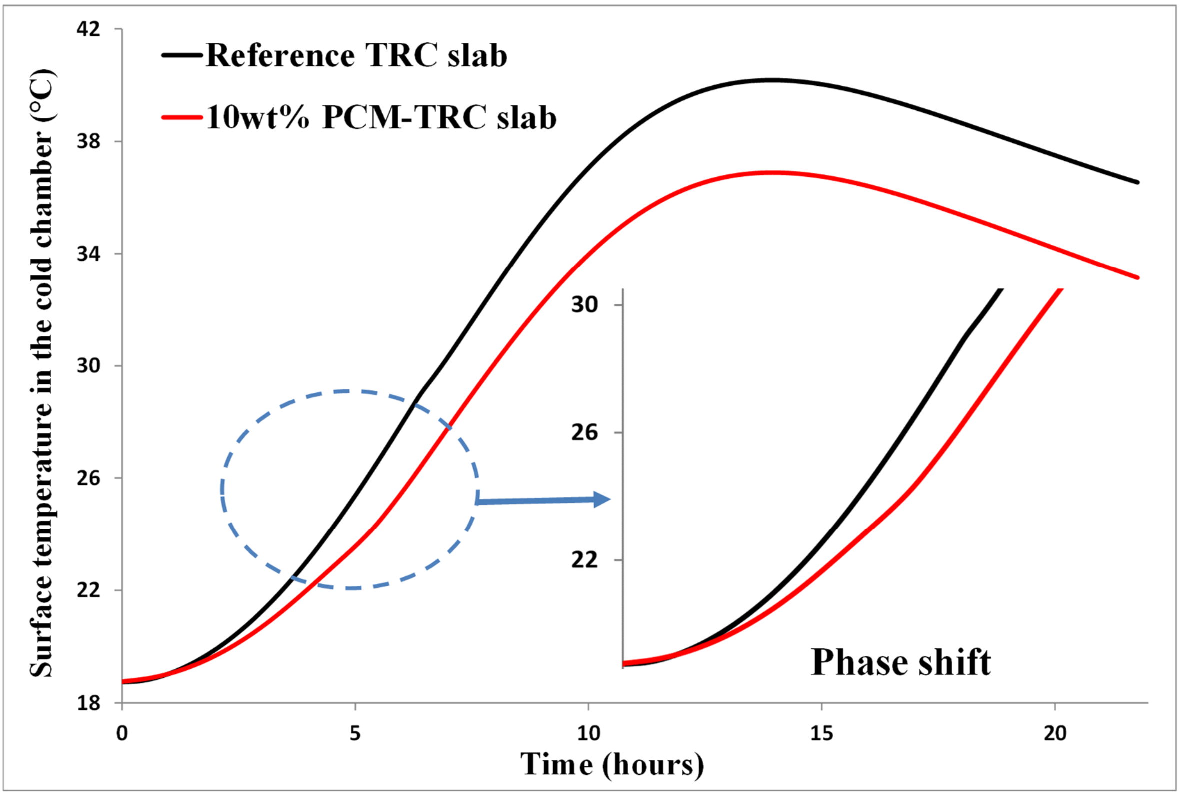

-a-

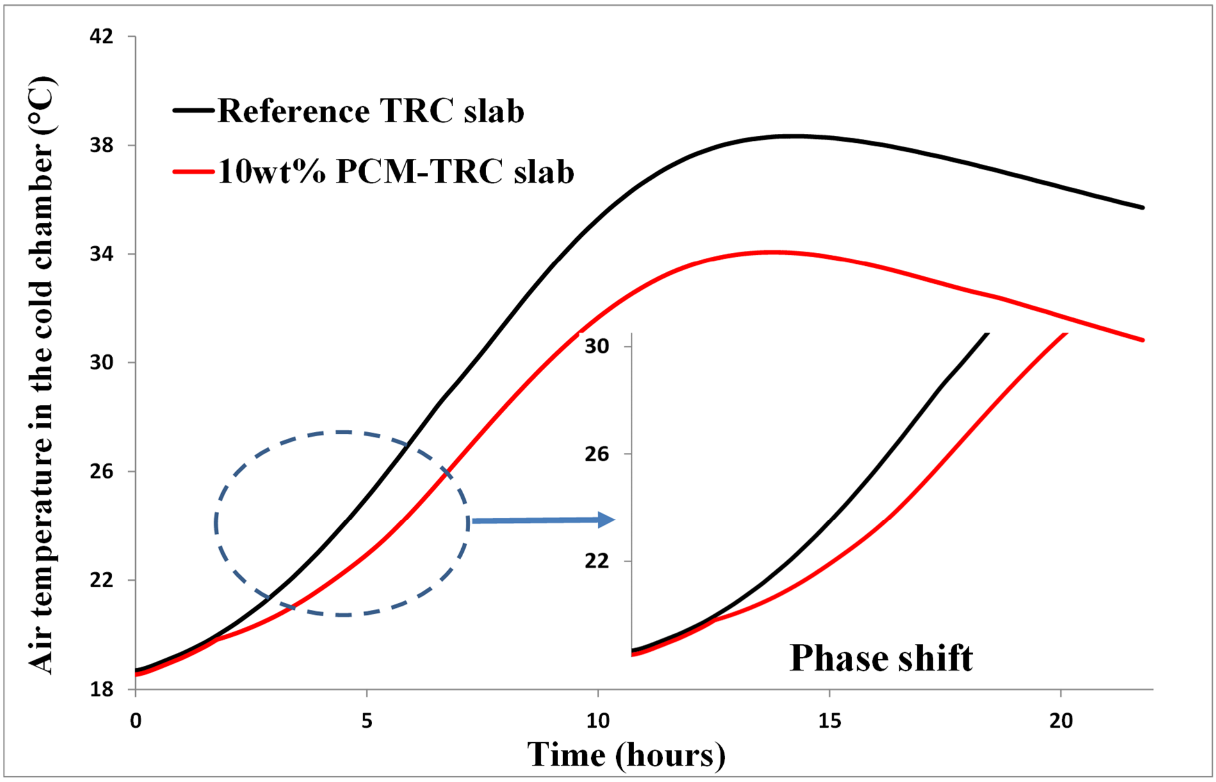

-b

Figure 20 –a samples surface temperature **–b-** Air temperature in the cold chamber

For the 10wt% PCM–TRC slab, the surface temperature in the cold chamber increased with an almost identical speed to that of the reference TRC slab in the 18.7–20°C temperature range. In contrast, when the surface temperature reached 22–27°C, a marked decrease in the speed of temperature increase was observed for the 10wt% PCM–TRC slab. This slowdown was due to the phase change (increase in specific heat of PCM and absorption of latent heat to induce phase change). The rate of temperature increase remained unchanged for the reference TRC slab.

The rate of air temperature increase in the cold chamber also demonstrated a slowing down trend in the temperature range of 20–25°C for the 10wt% PCM–TRC slab, whereas it remained unchanged for the reference TRC slab. The slight difference between the two ranges of occurrence of slowdown in temperature rise (between the indications of the surface temperature sensors and cold-side air temperature sensors) can be attributed to the heat transfer by convection from the surface of the sample to the interior air.

In comparison with the reference TRC slab during the heating process, the 10wt% PCM–TRC slab exhibited a lower surface temperature and lower air temperature at the peak. Reductions of 3.6°C in the surface temperature and 4°C in the indoor air temperature at the peak were observed. The analysis of temperature evolution also indicates a phase shift of temperature that can reach up to 3 h at the occurrence of phase change.

To compare the heat storage capacities of the reference TRC and 10wt% PCM–TRC slabs, an analysis of the heat fluxes entering the hot chamber and exiting the cold chamber for the two slabs was performed. The differences between the incoming and outgoing flux in each slab are depicted in **Figure 21.**

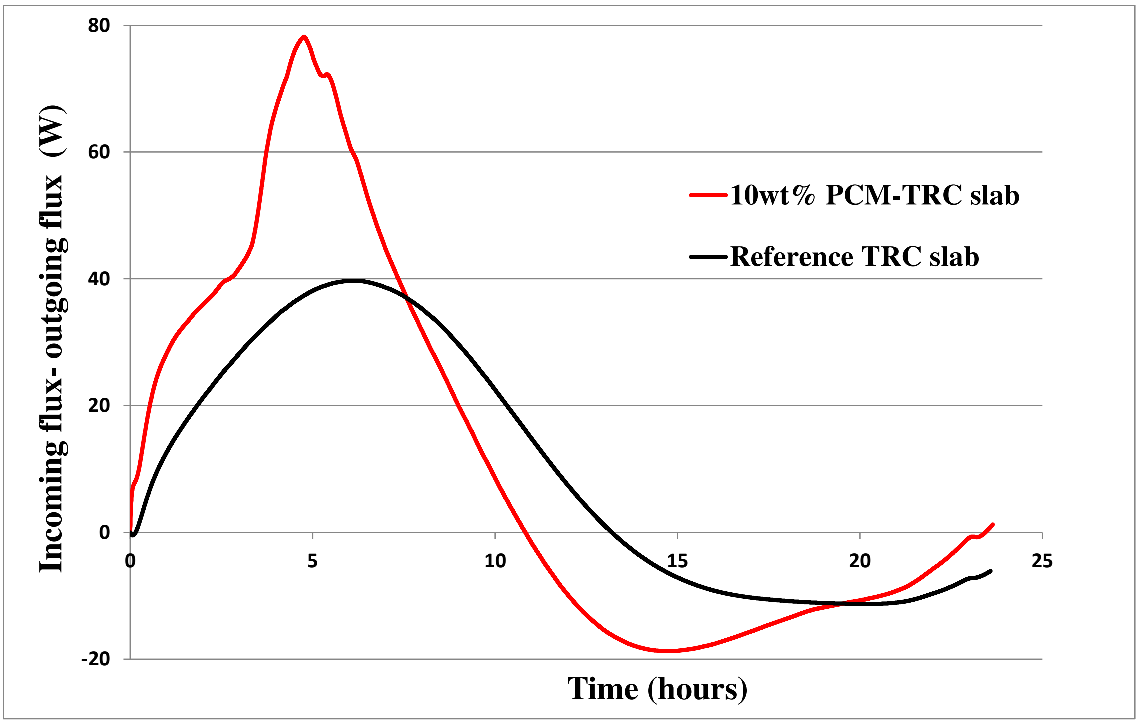

Figure 21 Flux analysis in the slabs

The energy stored for the two slabs was evaluated by integrating the difference between the incoming and outgoing flux over the heating time. The result for each configuration is presented in **Table 8**.

Energy reference slab (kJ)	Energy 10wt% PCM-TRC (kJ)	Energy gain
2340±42	3690±60	37%

Table 8 Heat storage in PCM-TRC slabs

It can be concluded after the analysis **of Figure 21** and **Table 8** that the 10wt% PCM–TRC slab presents an energy capacity gain of ~37% in comparison with the reference TRC slab. This is representing a similar gain (~37%) in terms of cooling cost (In fact, the proposed slab allows a passive use of the PCM (without the need of an energy consuming system to activate the PCM phase change). The energy capacity gain suggests that a significant part of the thermal storage capacity of the PCM is preserved, although damage occurs to some PCM capsules. This result is interesting for the future exploitation of the concept of PCM–TRC slabs. However, further studies are necessary to evaluate the efficiency of slabs on repetitive heating/cooling cycles (fatigue behavior).

‘Furthermore, for the assessment of the energy capacity of the PCM-TRC slabs in the case of a practical use, coupled evaluation (mechanical–thermal) should be investigated. In fact, the mechanical load applied on the slabs in the service state can affect the opening of cracks due to PCM phase change from solid to liquid which is likely to affect the thermal performance of the slabs'

3-Conclusion

This paper presents an innovative concept of a PCM–TRC slab that results from the association of a TRC composite with PCM microcapsules. The proposed concept is based on the idea of associating the lightweight specificity of TRCs with the thermal storage capacity of PCMs.

PCM–TRC composite slabs at different PCM rates were evaluated in terms of their mechanical and thermal performances. Based on the experimental design presented above, the following conclusions can be drawn:

-The increase in the PCM rate in the PCM–TRC slabs induced a degradation in their performance in terms of load-bearing capacity.

-The augmentation of the PCM rate in the slabs induced a degradation in the textile work ratio, and even led to a critical failure mode due to inferior matrix-to-textile bond conditions that induced textile slippage from the matrix for a PCM rate of 15wt%. This can be attributed to the disorders caused by PCM at the matrix/textile interface scale that induced a loss of bond matrix/textile.

Despite the degradation of the mechanical performance of the PCM–TRC slabs with increasing PCM content, the ductile and multicracking characteristics, as well as the matrix/textile stress transfer behavior, remained conserved. This allowed the PCM–TRC slabs to achieve load-bearing capacities at failure that were considerably greater than the force at the appearance of the first crack. This is particularly interesting for the future application of PCM–TRC slabs as load-bearing slabs.

The temperature and PCM state affect the mechanical performance of the PCM–TRC slabs. Bending tests conducted on 10% PCM–TRC slabs at temperatures of 20 and 40°C demonstrated that the 10wt% PCM–TRC slabs maintained and tested at 20°C exhibited a higher load-bearing capacity, as well as a higher textile work ratio, than those of the slabs that were heated to 40°C. This can be attributed to the cracks induced by the PCM during its phase change at the interface scale. These cracks disturb the stress transfer from the matrix to the interface until the textile reinforcement.

Further research can be undertaken to improve the mechanical performances of the PCM-TRC slab. For this purpose, the optimisation of the microcapsules content (raw PCM material, polymer shell of encapsulation) can be investigated to avoid the damage that can occur to PCM and its harmful consequences on the matrix behaviour. Another point that could be investigated, is using the pouring manufacturing technique for production of the PCM-TRC composites to avoid applying any pressure on PCM.

In terms of thermal performance, the thermal inertia of the 10 wt% PCM-TRC slab was evaluated in the guarded hot box. The thermal inertia tests indicated that the 10wt% PCM–

TRC slab attenuated the air temperature inside the cold chamber by 4°C in comparison with the reference TRC slab. The 10wt% PCM–TRC slab also allowed an increase of 37% in the heat storage capacity (representing a similar saving in terms of cooling cost). This suggests that a significant part of the thermal storage capacity of the PCM is preserved, although damage occurs to some PCM capsules.

The proposed concept of PCM-TRC slabs can be very promising for the future insulation of slabs in temperate climate where temperature conditions allows the PCM to ensure a full cycle of phase change (solid to liquid in the morning and liquid to solid in the night). However, further studies are necessary to evaluate the efficiency of the concept of PCM–TRC slabs on repetitive heating/cooling cycles

Appendix 1

All experimentally derived curves in the three points bending tests presented section 3-1-2-2 on three samples per PCM-TRC slab configuration (reference slab, 5wt% PCM-TRC slab, 10wt% PCM-TRC slab, 15wt% PCM-TRC slab) are presented below

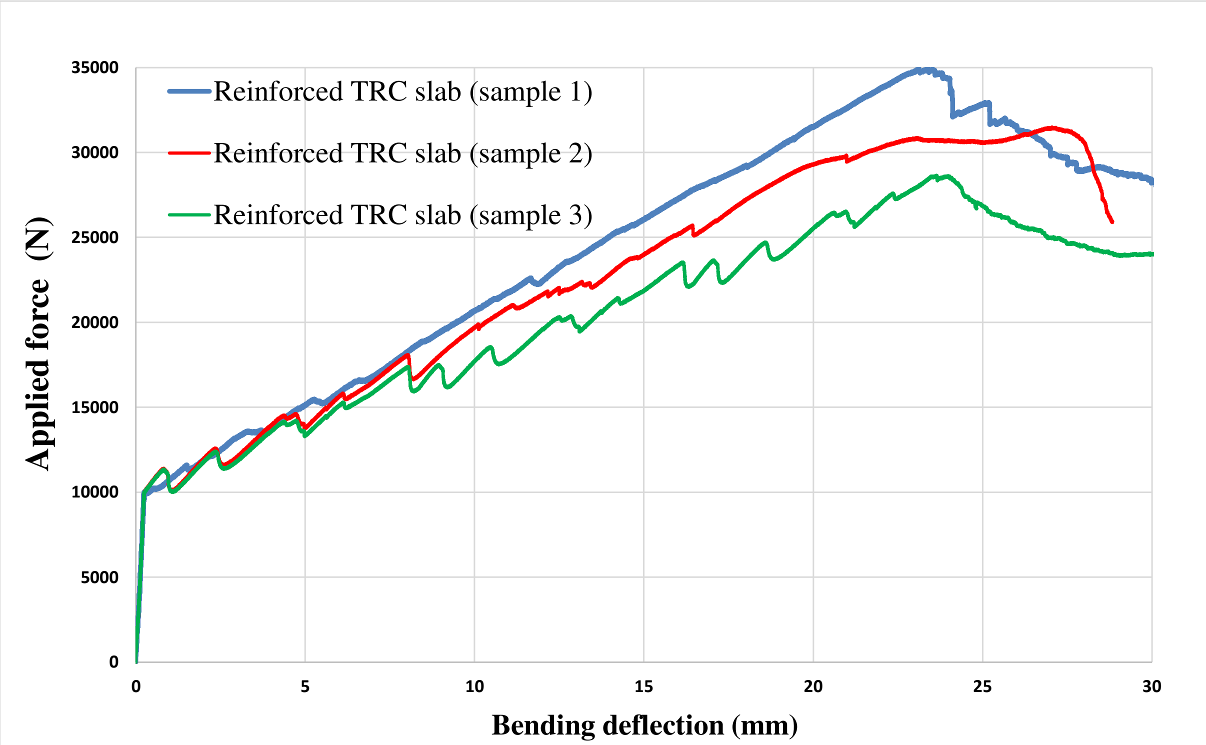

(a)

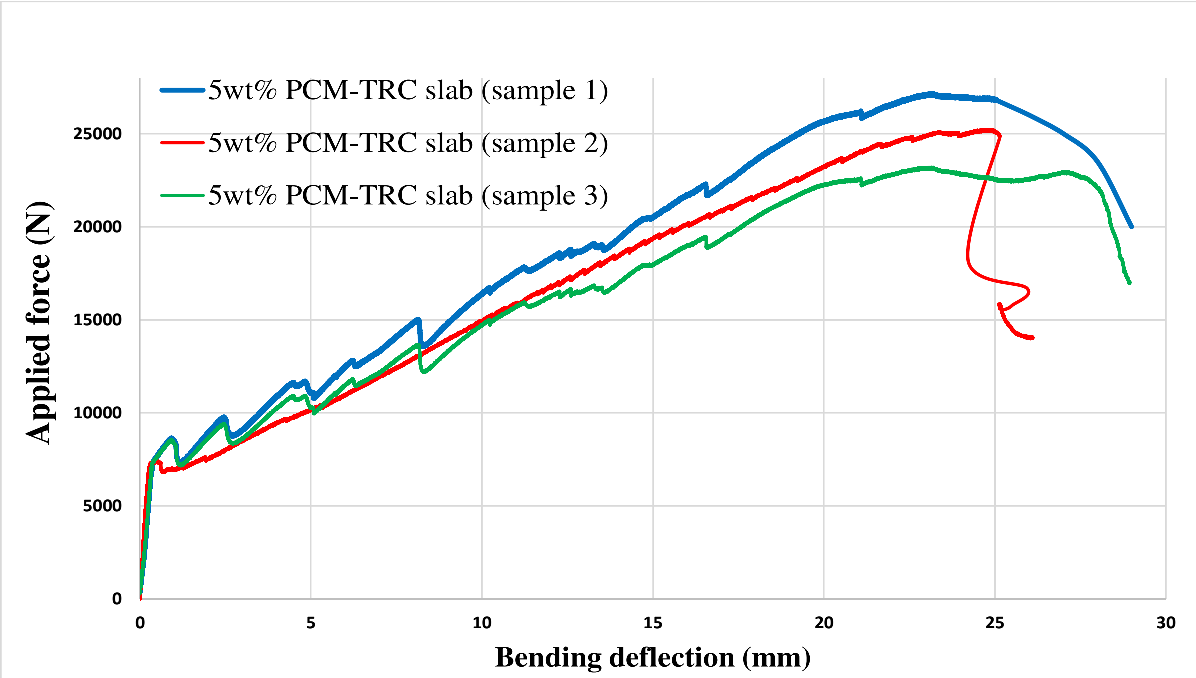
5wt% PCM-TRC slab (sample 1)
5wt% PCM-TRC slab (sample 2)
5wt% PCM-TRC slab (sample 3)
Applied force (N)
Bending deflection (mm)
0
5000
10000
15000
20000
25000
0
5
10
15
20
25
30

(b)

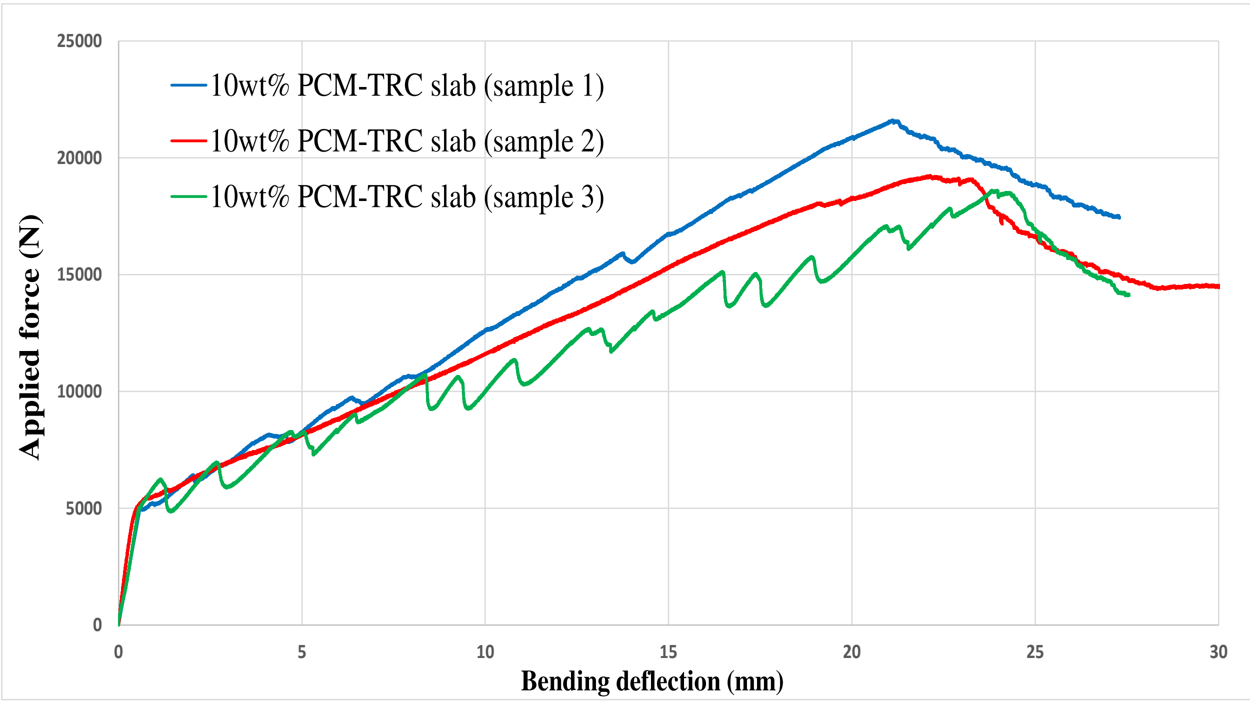
10wt% PCM-TRC slab (sample 1)
10wt% PCM-TRC slab (sample 2)
10wt% PCM-TRC slab (sample 3)
Applied force (N)
Bending deflection (mm)
0
5000
10000
15000
20000
25000
0
5
10
15
20
25
30

(c)

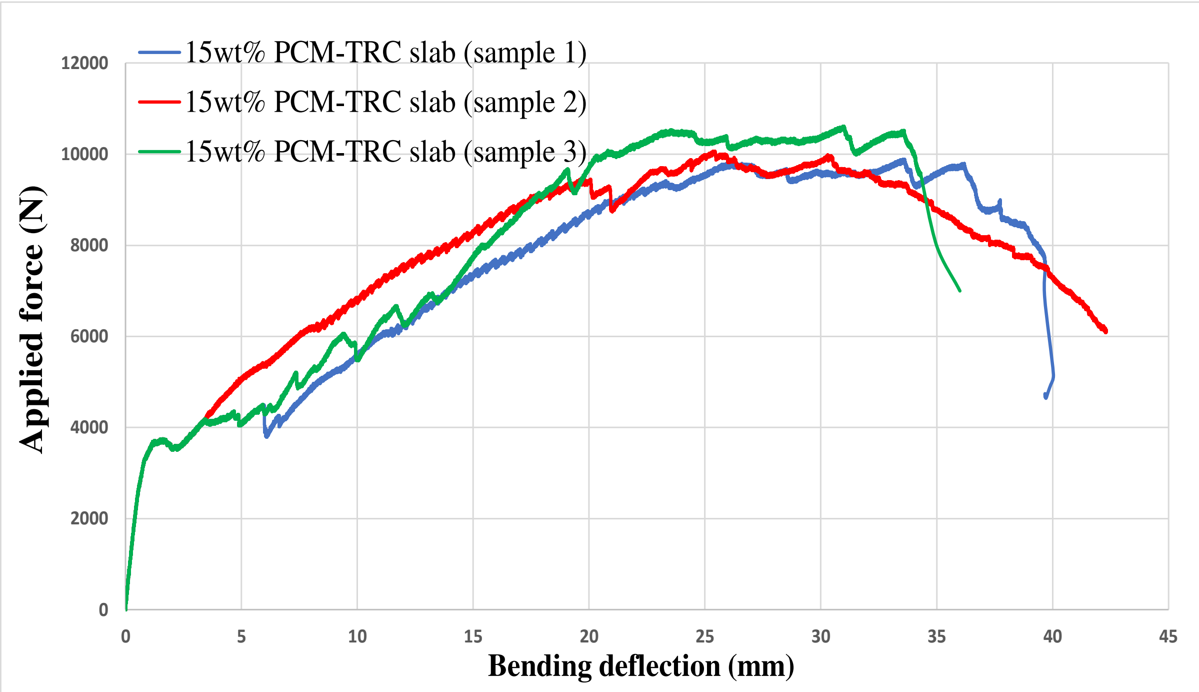

(d)

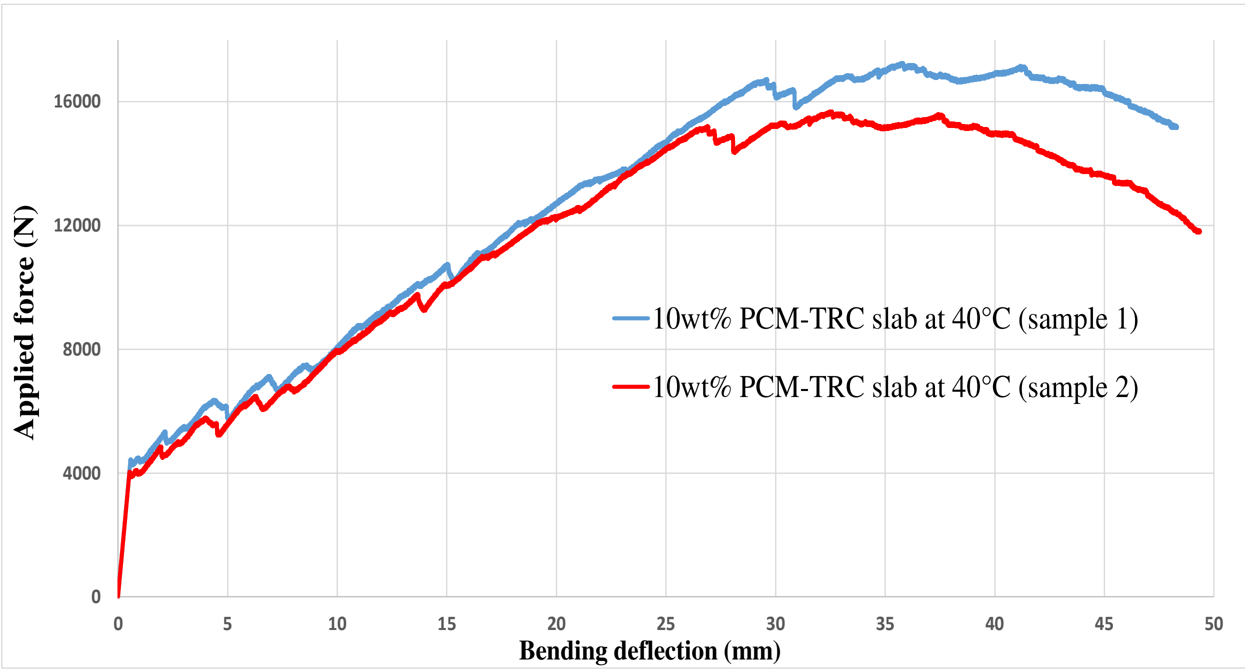

(d)

Figure 20 experimentally derived curves in the three points bending tests on (a) reference TRC slab (b) 5wt% PCM-TRC slab (c) 10wt% PCM-TRC slab (d) 15wt% PCM-TRC slab (e) 10wt% PCM-TRC slab at 40°C

Acknowledgement

.

The authors would like to warmly thank the company KAST (Sonthofen, Germany) for providing the textile reinforcement used in the study.

The authors also warmly thank Mr. Bernard Arnold (KAST) for his invaluable assistance

Conflicts of interests

The authors have no conflicts of interests to declare.

Funding:

This research is funded by the Vietnam National Foundation for Science and Technology Development (NAFOSTED) under grant number 107.01-2017.03.

The authors declare that they have no conflicts of interests.

Bibliography

[1] ADEME, les batiments à basse energie, retour d'experience en rhones alpes,2013.

[2] T D'Antino, C Papanicolaou, Mechanical characterization of textile reinforced inorganic-matrix composites, Composites Part B 127 (2017) 78-91

[3] Z Djamai, M Bahrar, F Salvatore, A Si Larbi, M El Mankibi, Textile reinforced concrete multiscale mechanical modelling: Application to TRC sandwich panels, Finite Elements in Analysis and Design 135 (2017) 21-35

[4] J Vervloet, P Van Iterbeek, S Verbruggen, M El Kadi, M De Munck, J Wastiels,T Tysmans, Experimental investigation of the buckling behaviour of Textile Reinforced Cement sandwich panels with varying face thickness using Digital Image Correlation, Construction and building materials, 51 (2014) 405-413

[5] A Shams, J Hegger, M Horstmann, An analytical model for sandwich panels made of textile reinforced concrete, Construction and Building Materials 64 (2014) 451-459

[6] I Colombo, M Colombo, M Di Prisco, Bending behavior of textile reinforced concrete sandwich beams, Construction and Building Materials 95 (2015) 675–685.

[7] Z I Djamai, K Erroussafi, A Si Larbi, F Salvatore, G Cai Analytical modeling of textile reinforced concrete (TRC) sandwich panels: Consideration of nonlinear behavior and failure modes, Mechanics of advanced Materials and structures (2020).

[8] J Vervloet, T Tysmans, M El Kadi, M De Munck, P Kapsalis, P Van Itterbeeck, J Wastiels, D Van Hemelerijck Experimental and numerical evaluation of textile reinforced cement (TRC) sandwich walls in compression: A geometrical study, Construction and building Materials 240 (2020) 1-11

[9] L Olivieri, J Tenorio, D Revuelta, L Navarro, L Cabeza, Developing a PCM-enhanced mortar for thermally active precast walls in Construction and Building Materials 181 (2018) 638-649

[10] M Pomnianowski, P heiselberg, R Jensen, R Cheng, Y Zhang, A new experimental method to determine specific heat capacity of inhomogeneous concrete material with incorporated microencapsulated –PCM, Cement and concrete research 55 (2014) 22-34.

[11] S Cunha, M Lima, J Aguiar, Influence of adding phase change materials on the physical and mechanical properties of cement mortars, Construction and Building Materials 127 (2016) 1–10

[12] L Boussaba, A Foufa, S Makhlouf, G Lefebvre, L Royon Elaboration and properties of a composite bio-based PCM for an application in building envelopes in Construction and building materials 185(2018) 156-165

[13] H W Min, S Kim, H S Kim, Investigation on thermal and mechanical characteristics of concrete mixed with shape stabilized phase change material for mix design, Construction and building materials 149 (2017) 749-762.

[14] D Zhang, Z Li, J Zhou, K Wu, Development of thermal energy storage concrete, Cement and Concrete Research 34 (2004) 927-934

[15] A Figueiredo, J Lapa, R Vicente, C Cardoso, Mechanical and thermal characterization of concrete with incorporation of microencapsulated PCM for applications in thermally activated slabs in Construction and Building Materials (2016) 126 332-344.

[16] Z Djamai, F Salvatore, A Si Larbi, G Cai, M El Mankibi, Multiphysics analysis of effects of encapsulated phase change materials (PCMs) in cement mortars, Cement and Concrete Research 119 (2019) 51-63.

[17] A Eddhahak-ouni, S Drissi, J colin, J Negi, S Carre, Experimental and multi-scale analysis of the thermal properties of Portland cement concretes embedded with microencapsulated phase change materials (PCMs), Applied thermal engineering 64 (2014) 32-39.

[18] E Mohseni, W Tang, S Wang Development of thermal energy storage lightweight structural cementitious composites by means of macro-encapsulated PCM, Construction and Building Materials 225 (2019)

[19] C Castellón, A Castell, M Medrano, I Martorell, L F.Cabeza Experimental Study of PCM Inclusion in Different Building Envelopes, Journal of Solar Energy Engineering 131(2009) 1-6

[20] M Hunger, A G Entrop, I Mandilaras, H J H Brookers, M Founti, The behavior of self-compacting concrete containing micro-encapsulated phase change Materials, Cement and Concrete Composites 31 (2009) 731–743

[21] A Thiele, A Jamet, G Sant, L Pilon, Annual energy analysis of concrete containing phase change materials for building envelopes in Energy conversion and management 103 (2015) 374-386.

[22] P K Dehdezi, M R Hall, A R Dawson, S P Casey, Thermal, mechanical and microstructural analysis of concrete containing microencapsulated phase change materials, Int. J. Pavement Eng. 14 (5) (2013) 449–462.

[23] V D Cao, S Pilehvar, C Salas-Bringas, A M Szczotok, Microencapsulated phase change materials for enhancing the thermal performance of Portland cement concrete and geopolymer concrete for passive building applications, Energy Conversion and Management 133 (2017) 56-66.

[24] N Esside, A Loulizi, J Naji Compressive strength and hygric properties of concretes incorporatingmicroencapsulated phase change material, Construction and building Materials 22 (2019), 254-262.

[25] M Aguayo, S Das, A Maroli, N Kabay, J Mertens, S Rajan, G Sant, N. Chawla, N. Neithalath, The influence of microencapsulated (PCM) characteristics on the microstructure and strength of cementitious composites: Experiments and finite element simulations, Cement and Concrete Composites 73 (2016) 29-41

[26] Z Djamai, A Si Larbi, F Salvatore, G Cai A new PCM-TRC composite: A mechanical and physicochemical investigation, Cement and Concrete Research 135 (2020) 106–119

[27] S Cunha**,** J Aguiar, V Ferreira, A Tadeu, A Garbacz Mortars with phase change materials - Part I: Physical and mechanical characterization*, Key* Engineering Materials 634 (2015) 22-32

[28] T Lecompte, P Le Bideau, P Glouannec, D Nortershauser, S Le Masson Mechanical and thermo-physical behaviour of concretes and mortars containing phase change material,Energy and buildings 94 (2015) 52-60

[29] B Savija, A Figueiredo, E Schlangen Influence of Microencapsulated Phase Change Material (PCM) Addition on (Micro) Mechanical Properties of Cement Paste, Materials 10 (2017)

[30] B Savija, M Lukovic, G Kotteman, S Figueredo, F de Mendoça Filho, E Schlangen Development of ductile cementitious composites incorporating microencapsulated phase change materials, International Journal of Advanced science and Applied Mathematics 9 (2017) 169-180

[31] S Pilehvara, V-D Cao, A M Szczotoka, L Valentinie Mechanical properties and microscale changes of geopolymer concrete and Portland cement concrete containing micro-encapsulated phase change materials, Cement and Concrete Research 100 (2017) 341-349

[32] S Pilehvar, S Sanfelix , A Szczotok, J Rodríguez, L Valentini, M Lanzón , R Pamies , A Kjøniksen Effect of temperature on geopolymer and Portland cement composites modified with Micro-encapsulated Phase Change materials

[33] Zakaria Ilyes DJAMAI Phd thesis Contribution à la caractérisation multi-échelle de composites textile mortier à inertie thermique renforcée par des matériaux à changement de phase (composite MCP-TRC) : application au bâtiment

[34] M Felix, J Aguiar Study of a cement mortar with incorporation of PCM microcapsules in proceeding of the 6th symposium of polymers in concrete, Shanghai China

[35] European norm: methods of testing cement. Determination of strength

[36] Test method for steady-state thermal performance of building assemblies by means of a guarded hot box